Statistical Model Criticism of Variational Auto-Encoders

Claartje Barkhof[1] **Wilker Aziz**[1]

[1]Institute for Logic, Language and Computation, University of Amsterdam

Abstract

We propose a framework for the statistical evaluation of variational auto-encoders (VAEs) and test two instances of this framework in the context of modelling images of handwritten digits and a corpus of English text. Our take on evaluation is based on the idea of statistical model criticism, popular in Bayesian data analysis, whereby a statistical model is evaluated in terms of its ability to reproduce statistics of an unknown data generating process from which we can obtain samples. A VAE learns not one, but two joint distributions over a shared sample space, each exploiting a choice of factorisation that makes sampling tractable in one of two directions (latent-to-data, data-to-latent). We evaluate samples from these distributions, assessing their (marginal) fit to the observed data and our choice of prior, and we also evaluate samples through a pipeline that connects the two distributions starting from a data sample, assessing whether together they exploit and reveal latent factors of variation that are useful to a practitioner. We show that this methodology offers possibilities for model selection qualitatively beyond intrinsic evaluation metrics and at a finer granularity than commonly used statistics can offer.

1 INTRODUCTION

Recent developments in deep learning and approximate probabilistic inference [Mnih and Gregor, 2014, Titsias and Lázaro-Gredilla, 2014, Kingma and Welling, 2014] have enabled the tractable estimation of flexible probabilistic models over complex sample spaces (*e.g.*, images [Kingma et al., 2016], natural language [Bowman et al., 2016], molecules [Simonovsky and Komodakis, 2018]). Deep or shallow, statistical models are seldom short of inadequacies [Theis et al., 2016]. Before a model can be assumed suitable to purpose, it is crucial that we criticise it along dimensions of relevance to the practitioner. Effective strategies for statistical model criticism [Box, 1980] require a combination of statistics and knowledge of the application domain, but methodology to assist in their design and automation does exist [Lloyd and Ghahramani, 2015]. This paper argues for the importance of statistical criticism in the context of deep probabilistic latent variable models (LVMs), in particular, one prominent class of deep LVMs—the variational auto-encoders [VAEs; Kingma and Welling, 2014]—introducing a methodology based on Bayesian estimation [Kruschke, 2013].

Lloyd and Ghahramani [2015] formulate criticism of a deep probabilistic model as a pipeline: choose a statistic, compute it for a data sample, use the probabilistic model as a null hypothesis and estimate a p-value in an attempt to reject the model. One of the main innovations in their design is to use the model itself as a null hypothesis, an idea with roots in Bayesian model checking [Gelman et al., 1996]. Their other innovation concerns the first step of this pipeline: instead of hand-picking a statistic, they chose a kernel and let maximum mean discrepancy [MMD; Gretton et al., 2012] find a statistic under which the two samples are maximally discrepant. Whether this *witness function* is even relevant will depend on the practitioner's ability to choose a good kernel. Altogether their strategy constrains model criticism to a binary decision (*i.e.*, is this model good under MMD or not?). Moreover, with a tool to find discrepancies in a rather flexible space of statistics, null falsification will eventually reject most models, for most models are imperfect along some view of the data. For criticism, we need tools that help uncover trade-offs of different models, rather than reject them as unable to account for the data's full complexity. Besides, we need tools that allow the analyst to control the degree of scrutiny that guides model comparison.

In this work, we derive a rich but low-dimensional statistic from the posterior predictive distribution of a latent structure model (*e.g.*, a hierarchical Bayesian model such as a Bayesian mixture model or latent Dirichlet allocation [Blei et al., 2003]). This model is chosen by the practitioner depending on the specific view of the data they expect (or need) their VAEs to capture. We also turn away from binary decisions and null hypothesis testing, instead comparing the statistics of different groups under a Bayesian mixed-membership model that allows for the comparison of multiple groups (*i.e.*, a control group and as many model groups as we have competing VAEs) and can answer complex queries regarding posterior discrepancy amongst groups. We motivate different dimensions of criticism relevant to the evaluation of VAEs and carefully design control groups that allow for comparing models along those dimensions. Finally, we demonstrate the application of this methodology in modelling the MNIST dataset [Deng, 2012] and the sentences in the English Penn Treebank [Marcus et al., 1993].

2 BACKGROUND

Estimation of a generative model involves associating a distribution p_X with a random variable X that captures an unknown data generating process q_X for which we have observations $\mathcal{D}_X = \{x^{(n)}\}_{n=1}^N$.[1] Commonly, we select from a parametric family the p_X whose likelihood given observations is maximum. Statistical criticism of p_X then involves determining whether *(i)* p_X approximates statistical properties of future data. In an LVM, p_X is the marginal of a joint distribution p_{XZ}, where Z is a latent variable. LVMs have various applications: a marginal may be more expressive than simple parametric families available, which can lead to better fit of the data; latent variables partition the probability space inducing clusters and/or other forms of potentially interpretable structure. In a directed LVM, we choose a prior distribution p_Z for the latent variable, which establishes its statistical and geometrical properties, and a conditional model $p_{X|Z=z}$ of the observed variable—the *observational model*. In addition to *(i)*, criticising an LVM involves determining whether *(ii)* the model reveals unobserved factors of variation (*i.e.*, hidden structure) that are useful to a practitioner. Whereas *(i)* concerns the fit of p_X to the unknown data generating process, *(ii)* concerns the perceived usefulness of inferences based on the generative model's posterior distribution $p_{Z|X=x}$. Crucially, *(ii)* hinges on the observational model's ability to exploit the latent space to explain unobserved factors of variation of data samples. Posterior inference for p_{XZ} is generally intractable, hence modern LVMs use auxiliary components for approximate inference, these introduce additional nuances to model criticism.

[1]**Notation:** we use capital letters (*e.g.*, X, Z) for random variables and lowercase letters (*e.g.*, x, z) for their assignments. For a random variable X, we use Ω_X to denote its domain and p_X to denote its distribution (with some abuse of notation, we also use p_X to denote the probability density function, but this should be unambiguous in context). Sometimes we need to refer to two distributions for the same random variable, each characterised by a different density function, in those cases we will use p_X and q_X.

VAEs [Kingma and Welling, 2014, Rezende et al., 2014] are directed LVMs that employ neural networks (NNs) to parameterise the observational model $p_{X|Z=z}$. This flexible parameterisation precludes marginal inference and thus standard gradient-based parameter estimation. VAEs resort to variational inference [VI; Jordan et al., 1999], and amortised VI [Kingma and Welling, 2014] in particular, to circumvent intractable posterior inference and enable tractable parameter estimation. Amortised VI involves choosing a joint distribution q_{ZX} determined by chaining an unknown data generating process q_X and a conditional model $q_{Z|X=x}$ of the latent variable—the *inference model*. Samples from the former are available through a dataset ($\mathcal{D}_X$), whereas the latter is a member of a tractable family parameterised by an NN and optimised along with the generative model p_{XZ} to approximate that model's posterior distribution via minimisation of $\mathbb{E}_{x\sim\mathcal{D}_X}[\mathrm{KL}(q_{Z|X=x}||p_{Z|X=x})]$. As a function of the inference model, the Kullback-Leibler divergence $\mathrm{KL}(q_{Z|X=x}||p_{Z|X=x})$ is independent of the marginal density $p_X(x)$, thus yielding a tractable objective for the estimation of $q_{Z|X=x}$. As a function of the observational model, this leads to a lowerbound $\mathbb{E}_{z\sim q_{Z|X=x}}[\log p_{X|Z=z}(x)] - \mathrm{KL}(q_{Z|X=x}||p_Z)$ on the model log-likelihood (the evidence lowerbound, ELBO), which we can use as a proxy for the estimation of $p_{X|Z=z}$. The inference model is a tool for tractable approximate inference, and in a VAE, it also enables estimation of p_{XZ}. Thus, the qualitative properties of $p_{Z|X=x}$ is affected by trade-offs we make in the specification of $q_{Z|X=x}$ (*e.g.*, factorisation assumptions), properties of the objective of optimisation (*e.g.*, KL divergence is asymmetric and, in the direction we use, it is lenient to underestimation of posterior variance), as well as our ability to optimise non-convex objective functions (*e.g.*, practical gradient-based optimisers offer at most local convergence). Even though p_{XZ} and q_{ZX} are meant to give two views of one probability space, these practical limitations lead the two spaces to diverge from one another. A necessary condition for their consistency is that their marginals match [Song and Ermon, 2020]. Thus, criticising a VAE further involves *(iii)* assessing the extent to which chaining its trainable components recovers q_X and p_Z in expectation.

3 INTRINSIC CRITICISM OF VAES

The most common intrinsic evaluation metric for density estimation is the log-likelihood (LL) of the model given a heldout sample of the data. The LL of a VAE is intractable, hence it is common to resort to Monte Carlo (MC) estimates through importance sampling [IS; Robert et al., 2004]. While importance weighted LL [IW LL; Burda et al., 2016] gives insight into the extent to which the marginal p_X matches the implicit distribution q_X on average (criterion *(i)*), it falls short in providing intuition for trade-offs made in the model regarding the usage of Z that we practically care about (criteria *(ii)* & *(iii)*).

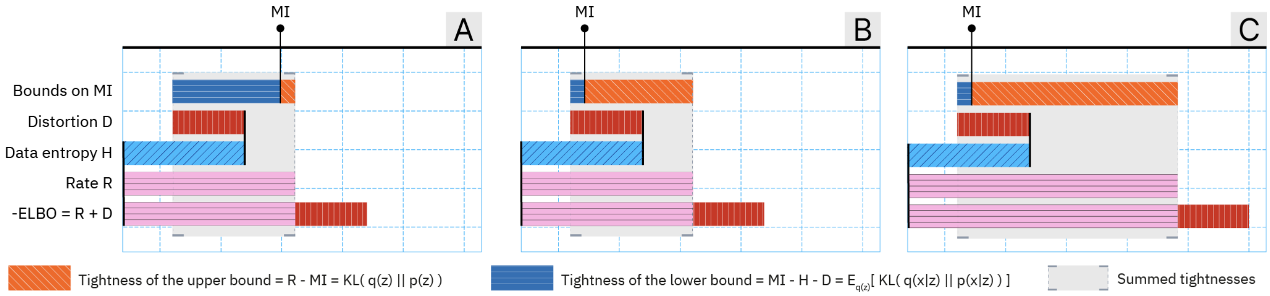

Figure 1: The diagrams illustrate three scenarios with different trade-offs in information theoretic quantities. Moving between scenario A and B keeps the ELBO, rate *and* distortion fixed, while the level of MI varies within the range defined by its variational bounds (denoted with the grey area). This variability allows for one scenario (B) to have a higher level of marginal KL relative to the other scenario (A). This illustrates that marginal KL is an axis of variation not accounted for in the information theoretic RD-view on VAEs. Moving from scenario B to C does *not* keep the RD-view (and thus ELBO) fixed and shows the potential hazardous situation where rate is elevated merely at the cost of marginal KL, without effectively diminishing distortion nor increasing MI. This scenario may seem predictably worse (after all, ELBO is worse), but it shows a caveat of techniques that focus on targeting higher rate solutions as a proxy to higher MI.

One example of a failure mode regarding criterion *(ii)* that need not be detected by IW LL is that of a model p_{XZ} in which the latent variable Z and observed variable X are independent. This has been reported to occur in cases where the observational model is flexible enough to model X without making use of Z, which establishes the consequence of a true posterior $p_{Z|X=x}$ that is independent of the data and is said to have *collapsed to the prior* [Chen et al., 2017, Bowman et al., 2016]. Due to this independence, VI finds a trivial optimum where $q_{Z|X=x}$ reduces to p_Z, perfectly recovering the collapsed $p_{Z|X=x}$ for every $x \in \Omega_X$. Motivated by this observation, Alemi et al. [2018] develop a view over the two axes the expected ELBO naturally decomposes into: the rate-distortion (RD) plane.[2] They demonstrate that these two quantities parametrically determine the unique variational bounds between which the mutual information (MI) between the observed variable X and latent variable Z under q_{ZX} is guaranteed to exist for a given parametric family. This leads to the insight that for any given ELBO level, the RD ratio may vary and so may the level of MI (quantitatively associated with criterion *(ii)*).

While the RD decomposition and its relation to the bounds on MI leads to an expanded intrinsic evaluation with regards to the goals outlined in Section 2, a closer look at these bounds reveals that there is a degree of freedom the decomposition through the lens of q_{ZX} does not account for, and which is directly relevant to criterion *(iii)*: q_Z matching p_Z. This can be quantified as the KL from the prior p_Z to the marginal q_Z [a.k.a. *marginal KL*; Hoffman and Johnson, 2016] and can be interpreted as the tightness of the upper-bound on MI, the rate, to the true MI. And, importantly, it may vary relative to the tightness of the lowerbound at fixed ELBO *and* fixed rate-distortion ratio (see Figure 1A & B). Furthermore, let us move from the theoretical situation where we reason in terms of fixed ELBO levels to a more realistic scenario where the optimal ELBO level at different RD ratios for a given parametric family is more likely to be defined by a bent RD-curve. In this scenario, the marginal KL may vary *independently* of the tightness of the lowerbound on MI. This is practically relevant as there are numerous optimisation techniques that directly or indirectly aim at solutions that lay on segments of or form points on the RD contour defined for a parametric family [e.g. Kingma et al., 2016, Pelsmaeker and Aziz, 2019, Chen et al., 2017, Alemi et al., 2018]. This thus potentially comes at the cost of compromised consistency and translates to higher marginal KL (Figure 1C). Considering a more complete view of RD together with marginal KL or MI can still lead to difficulties: it is hard to obtain good estimates of those quantities due to their dependence on the marginal q_Z, which is expensive to estimate and empirically bounded by $\log N$ [Song and Ermon, 2020]. On the other hand, even if we had perfect estimates at our disposal, reasoning on trade-offs between these quantities or proxies such as MMD is hard. And lastly–and possibly most importantly–none of these intrinsic metrics are explicitly designed to capture characteristics a practitioner may practically care about.

[2] The expected ELBO can be rewritten as $-D - R$, where $\mathbb{E}_{x \sim q_X}[\mathrm{KL}(q_{Z|X=x}||p_Z)]$ is the rate R and the distortion D is $\mathbb{E}_{x \sim q_X, z \sim q_{Z|X=x}}[\log p_{X|Z=z}(x)]$.

4 STATISTICAL CRITICISM FOR VAES

Our approach to comparing multiple VAEs is based on statistical criticism through Bayesian estimation [Kruschke, 2013, Benavoli et al., 2017]. We observe measurements from different groups of interest (*i.e.*, relevant statistics of data and/or model samples), some of which serve as control groups to help establish degrees of reasonable variation.

We posit a hierarchical model of all grouped measurements and infer a posterior distribution over its latent parameters. We then use the posterior distribution to visualise and/or quantify degrees of discrepancy between any model group and a control group, and use such summaries to, for example, order model groups in terms of resemblance to the control group. We have three criteria along which we criticise VAEs, namely, *(i)* 'does p_X fit the data?', *(ii)* 'is $p_{Z|X=x}$ practically useful', *(iii)* 'do p_{XZ} and q_{ZX} offer two views of the same probability space?'. Next, we describe our approach to comparing VAEs along these three dimensions.

Strategy. To criticise VAEs along criterion *(i)* we compare how a real-valued statistic $T(X)$ distributes as a function of data samples $x \sim q_X$ or model samples obtained by chaining the prior and the observational model ($\hat{x} \sim p_{X|Z=z}$ with $z \sim p_Z$). If $T(X)$ and $T(\hat{X})$ distribute similarly, then the VAEs correlate the variates in X at least in the way $T(\cdot)$ does. For criterion *(ii)*, we design a conditional statistic $T(X'|X)$ which has a structured view of (X, X') and compare how it distributes as a function of data samples $x' \sim q_X$ or model samples obtained by chaining the inference model and the observational model ($\tilde{x} \sim p_{X|Z=z}$ with $z \sim q_{Z|X=x}$) given a seed data sample $x \sim q_X$. If $T(X'|X)$ and $T(\tilde{X}|X)$ distribute similarly, the VAEs use latent space to correlate X and $\tilde{X}$ *at least* to the extent that $T(\cdot|\cdot)$ does. For criterion *(iii)*, we design two diagnostics. First, we go back to the unconditional statistic $T(X)$ and compare its distribution to that of $T(\tilde{X})$. Conditional model samples $\tilde{x}$ are model-based replications of seed samples, and, in expectation under q_X, they should reproduce patterns of the marginal p_X, no matter what the latent space is used for (or if it is used at all). Second, we turn to latent space, which, unlike Ω_X, is a (relatively) low-dimensional space, hence we compare prior samples ($z \sim p_Z$) to marginal samples ($\hat{z} \sim q_{Z|X=x}$ with $x \sim q_X$) directly.

Data samples. We assume availability of two collections drawn from q_X, one we shall call *training data* and denote $\mathcal{D}_X$, one we shall call *heldout data* and denote $\mathcal{H}_X$. Training data are called as such for they overlap with the data used for parameter estimation of the VAEs themselves. Both data sets are available for the comparison of VAEs, but, as VAEs are point-estimated using $\mathcal{D}_X$, heldout data help us assess their ability to generalise beyond training data.

Statistics. We use a real-valued statistic, rather than performing the analysis in data space directly, because it abstracts away from the high dimensionality of the data and because it can be made sensitive to a specific structured view of the data, one the practitioner is interested in. By the latter we mean, the practitioner is interested in models whose samples are indistinguishable from data samples at least through the lens of $T(\cdot)$ and/or whose latent spaces capture at least the structure that $T(\cdot|\cdot)$ is sensitive to. Concretely, we derive both statistics from the posterior distribution of a Bayesian latent structure model $\mathcal{S}$ whose modelling assumptions the practitioner controls. We condition on data samples available for the analysis (*e.g.*, $\mathcal{D}_X$) and expose their structure through the lens of the latent parameters of $\mathcal{S}$. Finally, for a future outcome x_*, $T(x_*)$ is the logarithm of the posterior predictive density (lppd) under $\mathcal{S}$: $T(x_*) =$

$$\log \int \sum_{c_*} p_{\text{samp}}(x_*|\phi, c_*) p_{\text{post}}(\phi, c_*|\mathcal{D}_X) \mathrm{d}\phi \ , \tag{1}$$

where p_{post} is the posterior of the analysis model, p_{samp} is that model's sampling distribution, ϕ is a global latent parameter and c is a local latent variable (typically discrete). This statistic can be thought of as a measure of discrepancy between a future outcome and the model $\mathcal{S}$—that is, the explicit modelling assumptions it makes and the data it conditions on. In practice we use a sampled estimate of the marginal probability. From the same model, we can derive the conditional statistic $T(\tilde{x}_*|x_*)$ of a replication $\tilde{x}_*$ of a seed sample $x_* \sim \mathcal{H}_X$ by assessing lppd under $\mathcal{S}$'s posterior distribution updated to also condition on the seed x_*: $T(\tilde{x}_*|x_*) =$

$$\log \int \sum_{c_*} p_{\text{samp}}(\tilde{x}_*|\phi, c_*) p_{\text{post}}(\phi, c_*|\mathcal{D}_X, x_*) \mathrm{d}\phi \ . \tag{2}$$

Bayesian estimation and model comparison. We are not interested in the magnitude of lppd as such, rather we aim at quantifying discrepancy in how this score distributes for each model group relative to a control group. As we shall see in Section 5, the statistics from different groups distribute in rather complex ways, thus, rather than fitting a simple parametric family (*e.g.*, a Student's t, as done in [Kruschke, 2013]), we use a Bayesian mixed-membership model [Blei, 2014, Airoldi et al., 2015] to jointly infer flexible density functions for all groups being analysed.

Let $\mathbf{y} \in \mathbb{R}^I_{>0}$ denote all measurements for the G groups in the analysis, each measurement being the negative of an outcome's lppd under $\mathcal{S}$. A grouped mixed-membership model samples the parameters of K components $(\mu_1, \sigma_1), \ldots, (\mu_K, \sigma_K)$ along with G vectors of mixing coefficients $\boldsymbol{\pi}_1, \ldots, \boldsymbol{\pi}_G$, each $\boldsymbol{\pi}_g \in \Delta_{K-1}$, from a Dirichlet process (DP) prior (*i.e.*, $K \to \infty$) with concentration $\alpha > 0$ and a base measure appropriate for the type of measurement. To model the negative of an outcome's lppd, we use a mixture of truncated Normal distributions $\mathcal{N}_+$ and our base measures are uniform over large subsets of the positive real line (details in appendix Section F). The likelihood function of the model is $\prod_{i=1}^I f(y_i|\boldsymbol{\pi}_{g_i}, \mu, \sigma)$, where $g_i \in \{1, \ldots, G\}$ indicates the group to which y_i belongs and $f(y|\boldsymbol{\pi}, \mu, \sigma) = \sum_{k=1}^K \pi_k \mathcal{N}_+(y|\mu_k, \sigma_k^2)$. To model latent variables directly, we use a mixture of low-rank multivariate Normal distributions and adjust the base measures accordingly (details in the appendix Section D).

Statistical discrepancy Our goal is to quantify discrepancy in distribution between groups of measurements $\{y_i : g_i = c\}$ and $\{y_i : g_i = m\}$, a control group c and a model group m, given measurements for all groups $\mathbf{y}$. For that we approximate the posterior KL divergence from the mixture $f_m(y_*) \triangleq f(y_*|\boldsymbol{\pi}_m, \mu, \sigma)$ to the mixture $f_c(y_*) \triangleq f(y_*|\boldsymbol{\pi}_c, \mu, \sigma)$: $\mathbb{E}[\mathrm{KL}(f_c||f_m)|\mathbf{y}] \leq$

$$\mathbb{E}[\mathrm{KL}(\mathrm{Categorical}(\boldsymbol{\pi}_c)||\mathrm{Categorical}(\boldsymbol{\pi}_m))|\mathbf{y}] \,, \quad (3)$$

where the KL between a mixture of shared components is upperbounded by the KL divergence between the distributions over component assignments [Hershey and Olsen, 2007]. We obtain an MCMC estimate of the expected value, for the DP we truncate a stick-breaking procedure at finite K. We make use of a No-U-Turn Sampler for improved efficiency [Hoffman et al., 2014]. For the analysis of Z we resort to SVI instead of MCMC.

5 EXPERIMENTS

In this section we demonstrate the use of the proposed statistical framework for evaluating a set of VAEs in the context of modelling a statically binarised version of MNIST [Deng, 2012] and the English PTB [Marcus et al., 1993].

5.1 VAES

Optimisation criteria. We employ three different optimisation criteria in our experiments that by design relate to the issues highlighted Section 3. **β-VAE** (BetaVae): Higgins et al. [2017] propose a framework for controlling the capacity of the information bottleneck by adding a hyperparameter β to the ELBO objective. **Info-VAE** (InfoVae): Zhao et al. [2018] propose this optimisation criterion to allow for explicitly controlling the balance between accurate posterior inference and maintaining substantial mutual information between the latent and observed variables. We implement this objective as a β-VAE objective with an additional MMD term, weighted with hyperparameters λ_{rate} and λ_{MMD} respectively. **Free bits VAE** (FbVae): to counteract the mutual information between the latent and observed variables to vanish and indirectly stimulate a non-collapsed posterior Kingma et al. [2016] propose to alter the expected ELBO replacing R by $\max(\lambda_{\text{FB}}, R)$ in an attempt to enforce a minimum rate. For both the experiments on MNIST and PTB we select a range of values for β, λ_{rate}, λ_{MMD} and λ_{FB}, which are listed together with an overview of the criteria in the supplementary material (Section B, Tables 2 and 1).

Architectures. For all experiments we implement a standard VAE with a fully factorised Gaussian approximate posterior $q_{Z|X=x}$ and a standard Gaussian as prior p_Z. The dimensionality of the latent space used across all the MNIST experiments is 10 and for all the PTB experiments 32. We describe some important architectural details below and refer the reader to Section C of the supplementary material for more details. **MNIST:** We experiment with two types of observational model. The simple model is a fully factorised product of Bernoulli distributions with gated transposed convolution layers as its main building block (*i.e.*, CNN.T decoder), following van den Berg et al. [2018]. The more complex observational model employs a conditional Pixel-CNN++ architecture [Salimans et al., 2017] to achieve an autoregressive product of Bernoulli distributions, following the implementation of Alemi et al. [2018]. We keep the architecture of the inference model (the *encoder*) fixed and again follow the implementation with gated convolutional layers of van den Berg et al. [2018]. **PTB:** We experiment with an auto-regressive factorisation of the observational model, and follow Li et al. [2020] in altering a transformer architecture [RoBERTa; Liu et al., 2019] to an auto-regressive model that incorporates the latent via two mechanisms: the embedding mechanism and the attention mechanism. To decrease computational overhead we initialise the weights with a distilled checkpoint [Sanh et al., 2019]. For the encoder we use an original version of the RoBERTa architecture initialised with the same distilled weights.

5.2 LATENT STRUCTURE MODELS

Here we describe the latent structure models (LSMs) used to assign lppd to the model samples and control groups outlined in Section 4. Their designs and complexity may vary across application domains and be chosen according to the practitioners liking, but we encourage to iteratively build complexity as even simple models can have surprising discriminative power, as we shall see. The graphical representations of our LSMs are shown in Table 3 in the supplementary material. It is worth noting that even though LSMs themselves are of generative nature, their ability to act as a generator in a realistic scenarios is simply too limited. But, their latent parameters may capture a data-driven notion of the latent structure at hand which a practitioner may want a more powerful generator, such as a VAE, to also induce. Moreover, if samples from a VAE do not seem data-like under the LSM's (simple) factorisation, the VAE has surely failed at modelling the complex q_X.

MNIST digit identiy model. The most obvious latent structure present in the MNIST dataset is that of the digit identity. Assessing whether VAEs capture this structure helps detect severely failed optimisation. To this end we design a simple LSM that is a mixture over 10 components, each of which is defined as a joint over independent Bernoulli distributions with a shared Beta prior to model the pixel values. This can be thought of as a naive Bayes classifier, and, in fact, we supervise it by pre-annotating the MNIST training data with classes predicted using a k-nn classifier (with 96.6% accuracy).

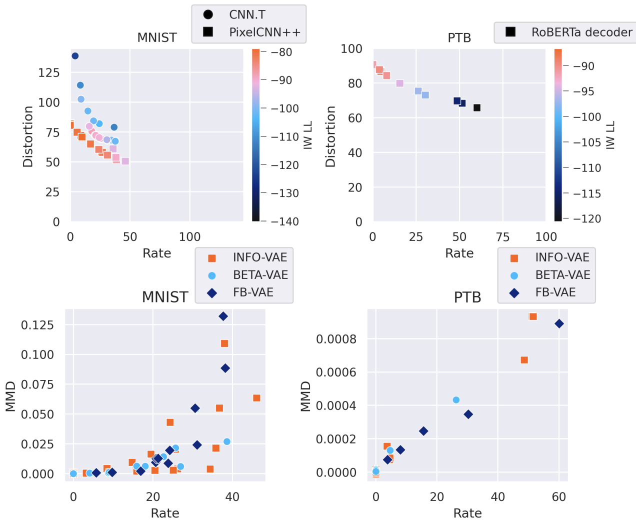

Figure 2: The intrinsic evaluation results of all experiments.

PTB sequence length model. A core property of written text is variability in sequence length. To test whether our VAEs capture this characteristic credibly, we design an LSM that models sentence length under a latent mixture of Poissons (latent components in Figure 7 of the supplement).

PTB topic model. Subsequently, we define another LSM to evaluate VAEs fitted on PTB which focuses more on the content of the written text. To this end, we use latent Dirichlet allocation [LDA; Blei et al., 2003] to uncover an underlying topic structure to the text we are modelling in the form of distributions over word count vectors.

5.3 ANALYSIS

Intrinsic evaluation. Intrinsic evaluation metrics are summarised visually for all experiments in Figure 2. Full tabular results can be found in the supplementary material (Section E). For the MNIST CNN.T experiments we see that the trade-off between R and D is defined by a bent curve: the first segment of the curve defines a region where D can be diminished with R efficiently (steep D decrease between experiments) and the second segment of the curve defines a region where the opposite is true. For the PixelCNN++ experiments and all the PTB experiments we observe more typical strong decoder behaviour where the conversion between R and D is an inefficient one for all levels of R that have been recorded in our experiments. In the lower two plots we can observe that for almost all experiments MMD increases with an increase in R. To which extent this happens differs per objective in the MNIST experiments, but for PTB it seems that all objectives act quite similarly in this regard. Additionally, we observe that the MMD scale is quite different for MNIST than for PTB, which makes it hard to tie practical judgements to the consequence of elevated MMD.

Negative lppd under latent structure model. To get an initial overview of the result of our analysis, we plot the histograms of the collected statistics for a subset of the experiments together with those belonging to the control group in Figure 3. We sort and colour the rows of the plots according to IW LL. Plots with all experiments can be found in the supplementary material (Section D). By inspecting the distributions we can make a few general observations. Primarily, it can be observed that the ordering according to IW LL does not generally correspond to the perceived divergences in histograms from the control group across statistics. On both ends of the IW LL spectrum we can find distributional discrepancies with respect to to the control group. Conversely, we can perceive differences in the distribution of statistics for models that are nearly identical in terms of IW LL. For the MNIST digit identity model (Figure 3a), for example, we can see that the best models in terms of statistics distributions seem to reside around an IW LL of -90. In fact, we can even distinguish models in that range by inspecting the histograms closely. We can, for example, distinguish them in their ability to model the multi-modal nature of the control group with regards to $T(X_*)$: the INFOVAE (2.0, 100) MNIST experiment seems to capture the small chunk of probability mass at the lower end of the spectrum better than the experiment above and below it. Similarly, for the PTB topic model (Figure 3c) we can for instance visually appreciate differences between the FBVAE (8.0) experiment and its row-wise neighbours, while they have nearly identical average IW LL estimates.

Posterior KL upperbound. Figure 4 is a summary of the analysis. It shows intrinsic evaluation metrics (1st column) alongside the estimated discrepancies relative to the control groups under the analysis models as described in Section 4 for a subset of the experiments. Full results can be found in the supplementary material Section G. The next three columns correspond to the discrepancies between distributions of the three lppd statistics in data space and the right-most column shows the discrepancy between prior samples and samples from the inference model averaged under $\mathcal{H}_X$. For the **digit identity model**, we can observe that low R models have a high average divergence to the data group in terms of the conditional statistic $T(\tilde{X}_*|X_*)$. This aligns with the intuition that these models fail to capture information on the digit identity in the latent space. Additionally, we can observe that increased R often coincides with larger discrepancy along the $T(X_*)$ and $T(\tilde{X}_*)$ statistics. On **PTB sequence length**, most models do not perform well in terms of encoding length in the latent space as recorded by the discrepancy along the $T(\tilde{X}_*|X_*)$ dimension, with the exception of high R models that seem to encode it to some extent. Models with low R (and collapsed posteriors) model length unconditionally as you might expect from large transformer based language models. The **PTB latent topics** paint a rather different picture. The tendency for high

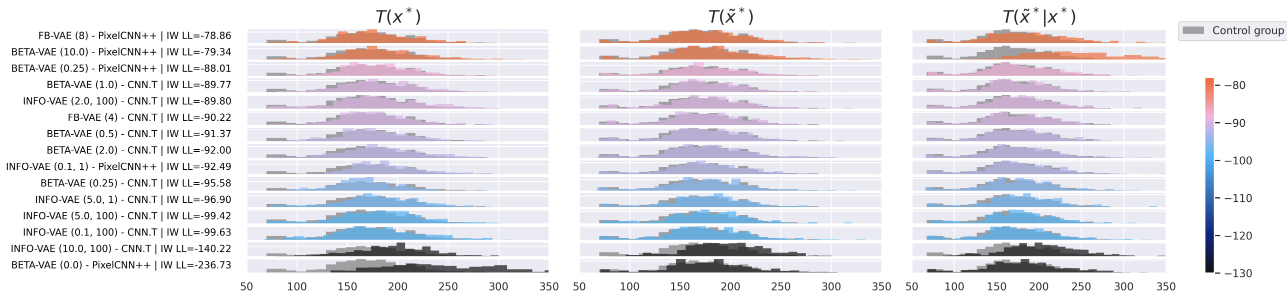

(a) MNIST digit identity

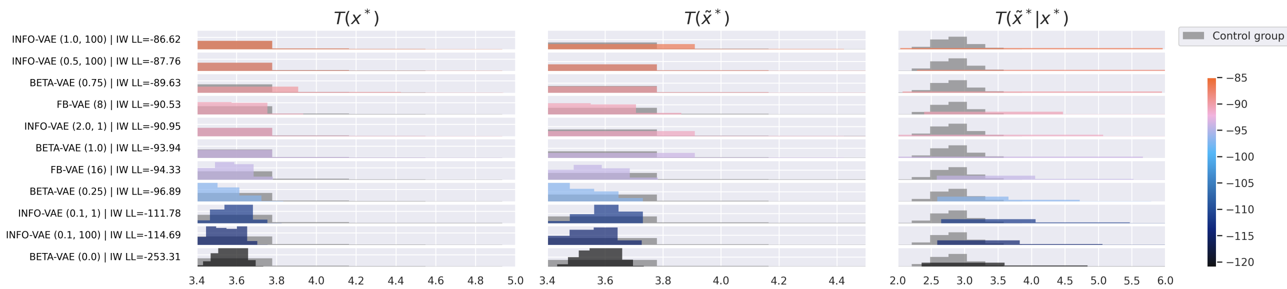

(b) PTB sequence length

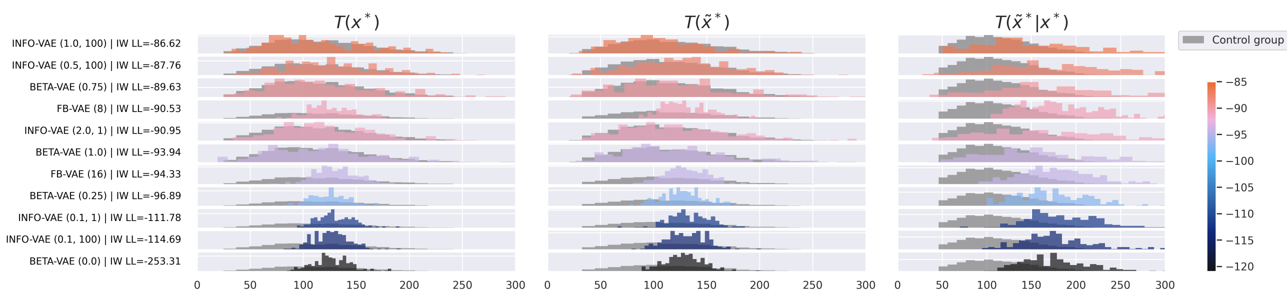

(c) PTB topics

Figure 3: The three statistics $T(X_*)$, $T(\tilde{X}_*)$ and $T(\tilde{X}_*|X_*)$ assessed under the three LSMs visualised for a subset of the experiments together with the distributions of the control groups. The rows are ordered and coloured by IW LL. The experiments are labelled with the objectives according to the following format: InfoVae (λ_{rate}, λ_{MMD}), BetaVae (β) and FbVae (λ_{FB}). For the MNIST experiments we additionally distinguish between decoder types used (CNN.T or PixelCNN++). We refer the reader for full experimental results to the supplementary material (Section D).

R and the conditional statistic $T(\tilde{X}_*|X_*)$ is flipped: higher R only harms along this axis and correspondingly along the other statistical axes.

For both MNIST and PTB, InfoVae with high enough λ_{MMD} weight can diminish divergence from the prior as measured by the latent analysis model. This does not, however, translate in consistent effects in the data space.

6 CONCLUSION

We have demonstrated the use of Bayesian data analysis techniques to criticise VAE in terms of the two probability distributions they prescribe. By employing LSMs that can be purpose chosen by a practitioner, we probe the VAEs for distributional compliance relative to a relevant control group. The lppd statistic is low-dimensional but reflects the LSM's richness, besides that it naturally accommodates a marginal and a conditional view, both crucial for analysing VAEs. We show that this methodology offers possibilities for model selection qualitatively beyond intrinsic evaluation metrics and at finer granularity than commonly used statistics can offer. Unlike NHST procedures, the components of our methodology are themselves amenable to model checking techniques, which help us build trust in the analysis. As our methodology interacts with the LVM only as a sampler, it can be extended to other LVMs such as GANs [Goodfellow et al., 2014] and diffusion models [Sohl-Dickstein et al., 2015, Kingma et al., 2021].

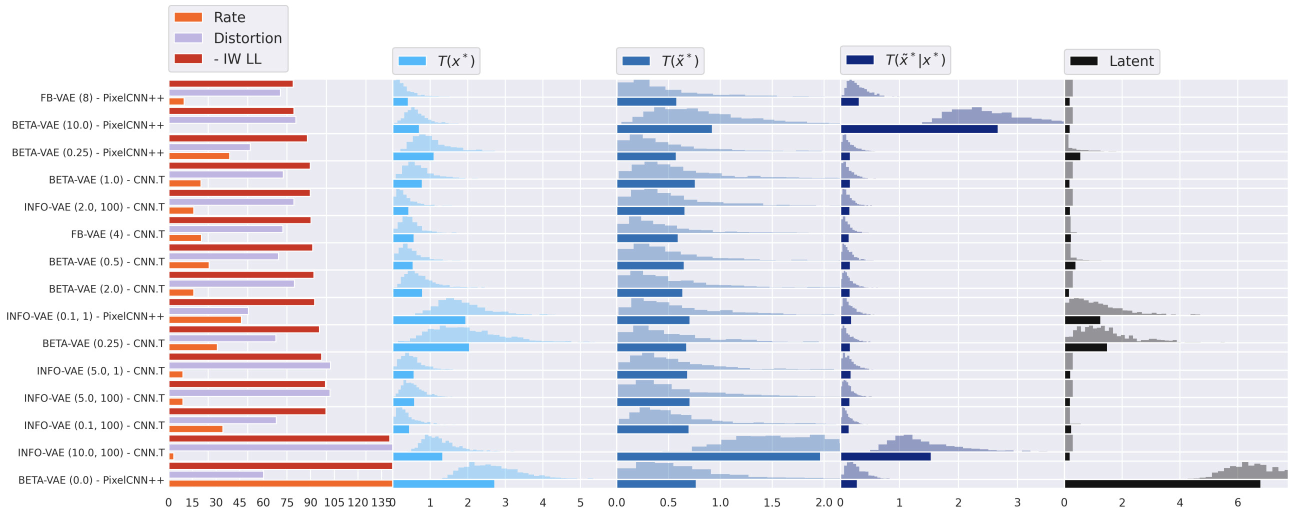

(a) MNIST digit identity

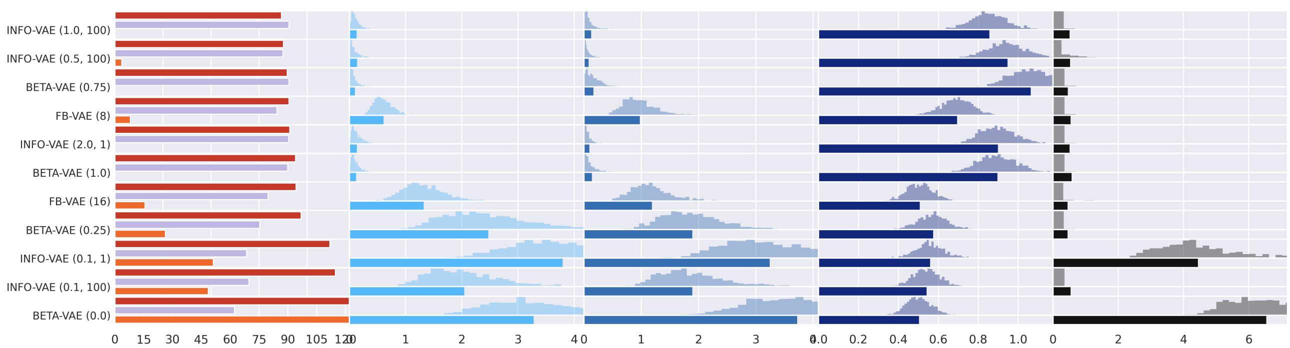

(b) PTB sequence length

(c) PTB topics

Figure 4: A summarising view of our analysis of a subset of the experiments. The leftmost column shows the intrinsic evaluation metrics for reference. The next three columns show estimated divergences from the control group under our analysis model. The rightmost column shows the estimated divergence from q_Z to p_Z. Full experimental results can be found in the supplementary material (Section G). The horizontal bars denote the average value of the sampled posterior divergences plotted as histograms. The experiments are labelled with the objectives according to the following format: INFOVAE (λ_{rate}, λ_{MMD}), BETAVAE (β) and FBVAE (λ_{FB}). For the MNIST experiments we additionally distinguish between decoder type used: CNN.T or PixelCNN++.

Acknowledgements

This project has received funding from the European Union's Horizon 2020 research and innovation programme under grant agreement No 825299 (GoURMET).

References

Edoardo M Airoldi, David M Blei, Elena Aleksandrovna Erosheva, and Stephen E Fienberg. *Handbook of mixed membership models and their applications*. CRC press, 2015.

Alexander Alemi, Ben Poole, Ian Fischer, Joshua Dillon, Rif A Saurous, and Kevin Murphy. Fixing a broken ELBO. In *International Conference on Machine Learning*, pages 159–168, 2018.

Alessio Benavoli, Giorgio Corani, Janez Demšar, and Marco Zaffalon. Time for a change: a tutorial for comparing multiple classifiers through bayesian analysis. *The Journal of Machine Learning Research*, 18(1):2653–2688, 2017.

Eli Bingham, Jonathan P Chen, Martin Jankowiak, Fritz Obermeyer, Neeraj Pradhan, Theofanis Karaletsos, Rohit Singh, Paul Szerlip, Paul Horsfall, and Noah D Goodman. Pyro: Deep universal probabilistic programming. *The Journal of Machine Learning Research*, 20(1):973–978, 2019.

David M Blei. Build, compute, critique, repeat: Data analysis with latent variable models. *Annual Review of Statistics and Its Application*, 1:203–232, 2014.

David M Blei, Andrew Y Ng, and Michael I Jordan. Latent dirichlet allocation. *Journal of machine Learning research*, 3(Jan):993–1022, 2003.

Samuel R. Bowman, Luke Vilnis, Oriol Vinyals, Andrew Dai, Rafal Jozefowicz, and Samy Bengio. Generating sentences from a continuous space. In *Proceedings of The 20th SIGNLL Conference on Computational Natural Language Learning*, pages 10–21, Berlin, Germany, August 2016. Association for Computational Linguistics.

George EP Box. Sampling and Bayes' inference in scientific modelling and robustness. *Journal of the Royal Statistical Society: Series A (General)*, 143(4):383–404, 1980.

Yuri Burda, Roger Grosse, and Ruslan Salakhutdinov. Importance weighted autoencoders. In *International Conference on Learning Representations*, 2016.

Xi Chen, Diederik P Kingma, Tim Salimans, Yan Duan, Prafulla Dhariwal, John Schulman, Ilya Sutskever, and Pieter Abbeel. Variational lossy autoencoder. In *International Conference on Machine Learning*, 2017.

Li Deng. The mnist database of handwritten digit images for machine learning research. *IEEE Signal Processing Magazine*, 29(6):141–142, 2012.

Andrew Gelman, Xiao-Li Meng, and Hal Stern. Posterior predictive assessment of model fitness via realized discrepancies. *Statistica sinica*, pages 733–760, 1996.

Ian Goodfellow, Jean Pouget-Abadie, Mehdi Mirza, Bing Xu, David Warde-Farley, Sherjil Ozair, Aaron Courville, and Yoshua Bengio. Generative adversarial nets. *Advances in neural information processing systems*, 27, 2014.

Arthur Gretton, Karsten M Borgwardt, Malte J Rasch, Bernhard Schölkopf, and Alexander Smola. A kernel two-sample test. *The Journal of Machine Learning Research*, 13(1):723–773, 2012.

Charles R. Harris, K. Jarrod Millman, Stéfan J. van der Walt, Ralf Gommers, Pauli Virtanen, David Cournapeau, Eric Wieser, Julian Taylor, Sebastian Berg, Nathaniel J. Smith, Robert Kern, Matti Picus, Stephan Hoyer, Marten H. van Kerkwijk, Matthew Brett, Allan Haldane, Jaime Fernández del Río, Mark Wiebe, Pearu Peterson, Pierre Gérard-Marchant, Kevin Sheppard, Tyler Reddy, Warren Weckesser, Hameer Abbasi, Christoph Gohlke, and Travis E. Oliphant. Array programming with NumPy. *Nature*, 585 (7825):357–362, September 2020.

John R Hershey and Peder A Olsen. Approximating the kullback leibler divergence between gaussian mixture models. In *2007 IEEE International Conference on Acoustics, Speech and Signal Processing-ICASSP'07*, volume 4, pages IV–317. IEEE, 2007.

Irina Higgins, Loic Matthey, Arka Pal, Christopher Burgess, Xavier Glorot, Matthew Botvinick, Shakir Mohamed, and Alexander Lerchner. beta-VAE: Learning basic visual concepts with a constrained variational framework. In *International Conference on Learning Representations*, 2017.

Matthew D Hoffman and Matthew J Johnson. ELBO surgery: yet another way to carve up the variational evidence lower bound. In *Workshop in Advances in Approximate Bayesian Inference, NeurIPS*, volume 1, 2016.

Matthew D Hoffman, Andrew Gelman, et al. The no-u-turn sampler: adaptively setting path lengths in hamiltonian monte carlo. *J. Mach. Learn. Res.*, 15(1):1593–1623, 2014.

MichaelI. Jordan, Zoubin Ghahramani, TommiS. Jaakkola, and LawrenceK. Saul. An introduction to variational methods for graphical models. *Machine Learning*, 37(2): 183–233, 1999.

Diederik P. Kingma and Max Welling. Auto-encoding variational bayes. In *International Conference on Learning Representations*, 2014.

Diederik P Kingma, Tim Salimans, Ben Poole, and Jonathan Ho. Variational diffusion models. *arXiv preprint arXiv:2107.00630*, 2021.

Durk P Kingma, Tim Salimans, Rafal Jozefowicz, Xi Chen, Ilya Sutskever, and Max Welling. Improved variational inference with inverse autoregressive flow. *Advances in neural information processing systems*, 29:4743–4751, 2016.

John K Kruschke. Bayesian estimation supersedes the t test. *Journal of Experimental Psychology: General*, 142(2): 573, 2013.

Chunyuan Li, Xiang Gao, Yuan Li, Baolin Peng, Xiujun Li, Yizhe Zhang, and Jianfeng Gao. Optimus: Organizing sentences via pre-trained modeling of a latent space. *arXiv preprint arXiv:2004.04092*, 2020.

Yinhan Liu, Myle Ott, Naman Goyal, Jingfei Du, Mandar Joshi, Danqi Chen, Omer Levy, Mike Lewis, Luke Zettlemoyer, and Veselin Stoyanov. Roberta: A robustly optimized bert pretraining approach. *arXiv preprint arXiv:1907.11692*, 2019.

James R Lloyd and Zoubin Ghahramani. Statistical model criticism using kernel two sample tests. In C. Cortes, N. Lawrence, D. Lee, M. Sugiyama, and R. Garnett, editors, *Advances in Neural Information Processing Systems*, volume 28. Curran Associates, Inc., 2015.

Mitchell P. Marcus, Beatrice Santorini, and Mary Ann Marcinkiewicz. Building a large annotated corpus of English: The Penn Treebank. *Computational Linguistics*, 19(2): 313–330, 1993.

Andriy Mnih and Karol Gregor. Neural variational inference and learning in belief networks. In *International Conference on Machine Learning*, ICML'14, pages II–1791–II–1799. JMLR.org, 2014.

Adam Paszke, Sam Gross, Francisco Massa, Adam Lerer, James Bradbury, Gregory Chanan, Trevor Killeen, Zeming Lin, Natalia Gimelshein, Luca Antiga, Alban Desmaison, Andreas Kopf, Edward Yang, Zachary DeVito, Martin Raison, Alykhan Tejani, Sasank Chilamkurthy, Benoit Steiner, Lu Fang, Junjie Bai, and Soumith Chintala. Pytorch: An imperative style, high-performance deep learning library. In H. Wallach, H. Larochelle, A. Beygelzimer, F. d'Alché-Buc, E. Fox, and R. Garnett, editors, *Advances in Neural Information Processing Systems 32*, pages 8024–8035. Curran Associates, Inc., 2019.

F. Pedregosa, G. Varoquaux, A. Gramfort, V. Michel, B. Thirion, O. Grisel, M. Blondel, P. Prettenhofer, R. Weiss, V. Dubourg, J. Vanderplas, A. Passos, D. Cournapeau, M. Brucher, M. Perrot, and E. Duchesnay. Scikit-learn: Machine learning in Python. *Journal of Machine Learning Research*, 12:2825–2830, 2011.

Tom Pelsmaeker and Wilker Aziz. Effective estimation of deep generative language models. *arXiv preprint arXiv:1904.08194*, 2019.

Du Phan, Neeraj Pradhan, and Martin Jankowiak. Composable effects for flexible and accelerated probabilistic programming in numpyro. *arXiv preprint arXiv:1912.11554*, 2019.

Danilo Jimenez Rezende, Shakir Mohamed, and Daan Wierstra. Stochastic backpropagation and approximate inference in deep generative models. In Eric P. Xing and Tony Jebara, editors, *International Conference on Machine Learning*, volume 32 of *Proceedings of Machine Learning Research*, pages 1278–1286, Bejing, China, 22–24 Jun 2014. PMLR.

Christian P Robert, George Casella, and George Casella. *Monte Carlo statistical methods*, volume 2. Springer, 2004.

Tim Salimans, Andrej Karpathy, Xi Chen, and Diederik P Kingma. Pixelcnn++: Improving the pixelcnn with discretized logistic mixture likelihood and other modifications. *arXiv preprint arXiv:1701.05517*, 2017.

Victor Sanh, Lysandre Debut, Julien Chaumond, and Thomas Wolf. Distilbert, a distilled version of bert: smaller, faster, cheaper and lighter. *ArXiv*, abs/1910.01108, 2019.

Martin Simonovsky and Nikos Komodakis. Graphvae: Towards generation of small graphs using variational autoencoders. In *International conference on artificial neural networks*, pages 412–422. Springer, 2018.

Jascha Sohl-Dickstein, Eric Weiss, Niru Maheswaranathan, and Surya Ganguli. Deep unsupervised learning using nonequilibrium thermodynamics. In *International Conference on Machine Learning*, pages 2256–2265. PMLR, 2015.

Jiaming Song and Stefano Ermon. Understanding the limitations of variational mutual information estimators. In *International Conference on Learning Representations*, 2020.

Lucas Theis, Aäron van den Oord, and Matthias Bethge. A note on the evaluation of generative models. In *ICLR*, 2016.

Michalis K. Titsias and Miguel Lázaro-Gredilla. Doubly stochastic variational bayes for non-conjugate inference. In *International Conference on Machine Learning*, pages 1971–1979, 2014.

Rianne van den Berg, Leonard Hasenclever, Jakub Tomczak, and Max Welling. Sylvester normalizing flows for variational inference. In *proceedings of the Conference on Uncertainty in Artificial Intelligence (UAI)*, 2018.

Shengjia Zhao, Jiaming Song, and Stefano Ermon. InfoVAE: Information maximizing variational autoencoders. In *Theoretical Foundations and Applications of Deep Generative Models*, ICML18, 2018.

A ACKNOWLEDGEMENTS TO OPEN-SOURCE SOFTWARE PROJECTS

We would like to give credit to some essential software projects we used extensively for our work. We would like to at least name Pyro [Bingham et al., 2019], NumPyro [Phan et al., 2019], Numpy [Harris et al., 2020], PyTorch [Paszke et al., 2019] and Scikit Learn [Pedregosa et al., 2011] as essential tool boxes for the experiments we have conducted and the analyses we have performed.

B EXPERIMENTAL SET-UP

B.1 OBJECTIVES

An overview of the objectives used in the experiments as described in Section 5 is given in Table 1. The hyperparameter settings of the separate runs are summarised in Table 2. The total number of experiments ran on the Penn Treebank dataset is 23 and on binarised MNIST 66.

Objective (hyperparameters)	Equation
β-VAE Higgins et al. [2017] (β)	$\max_{\theta,\phi} \mathcal{L}_{\beta\text{-VAE}}(\theta,\phi) = \mathbb{E}_{q_{Z\|X=x}}[\log p_{X\|Z=z}(\phi)] - \beta\,\mathrm{KL}(q_{Z\|X=x}(\theta)\|\|p_Z(\phi))$
Info-VAE Zhao et al. [2018] (λ_{rate}, λ_{MMD})	$\max_{\theta,\phi} \mathcal{L}_{\text{Info-VAE}}(\theta,\phi) = \mathbb{E}_{q_{Z\|X=x}}[\log p_{X\|Z=z}(\phi)] - \lambda_{\text{rate}}\,\mathrm{KL}(q_{Z\|X=x}(\theta)\|\|p_Z(\phi)) + \lambda_{\text{MMD}}\mathrm{MMD}$
Free-bits-VAE Kingma et al. [2016] (λ_{FB})	$\max_{\theta,\phi} \mathcal{L}_{\text{FB-VAE}}(\theta,\phi) = \mathbb{E}_{q_{Z\|X=x}}[\log p_{X\|Z=z}(\phi)] - \max(\mathrm{KL}(q_{Z\|X=x}(\theta)\|\|p_Z(\phi)), \lambda_{\text{FB}})$

Table 1: Overview of the objectives with their hyperparameters used for the experiments.

	PTB	MNIST
$\beta \in$	$\{0.0, 0.25, 0.5, 0.75, 1.0, 2.0\}$	$\{0.0, 0.25, 0.5, 0.75, 1.0, 1.5, 2.0, 5.0, 10.0\}$
$(\lambda_{\text{rate}}, \lambda_{\text{MMD}}) \in$	$\{1, 10, 100\} \times \{0.1, 0.5, 1.0, 2.0\}$	$\{1, 10, 100\} \times \{0.1, 0.5, 1.0, 2.0, 5.0, 10.0\}$
$\lambda_{\text{FB}} \in$	$\{4, 8, 16, 32, 64\}$	$\{4, 8, 16, 24, 32, 40\}$

Table 2: The hyperparameters for the objectives outlined in Section 5

.

C ARCHITECTURES

C.1 BINARISED MNIST

C.1.1 Gated CNN Encoder

We use the the gated convolutional encoder from van den Berg et al. [2018] with two additional linear layers to map to the location and scale parameters of the approximate posterior. The gating mechanism can be expressed as follows, where $*$ denotes convolution and $\odot$ denotes element-wise multiplication:

$$\mathbf{y}_{\text{GatedConv2D}} = (\mathbf{V} * \mathbf{x} + \mathbf{b}) \odot \sigma(\mathbf{W} * \mathbf{x} + \mathbf{c})$$

The encoder consists of the following GatedConv2d layers, with the parameters between parentheses denoting number of input channels, number of output channels, kernel size, stride and padding respectively:

- GatedConv2d(1, 32, 5, 1, 2)
- GatedConv2d(32, 32, 5, 2, 2))
- GatedConv2d(32, 64, 5, 1, 2)
- GatedConv2d(64, 64, 5, 2, 2)
- GatedConv2d(64, 64, 5, 1, 2)
- GatedConv2d(64, 256, 7, 1, 0)

C.1.2 Gated CNN.T decoder

Similarly, for the simple decoder architecture we follow van den Berg et al. [2018] by using GatedConvTranspose2d units as the main building block to map the sampled latent representation $\mathbf{z}$ to the parameters of Bernoulli distributions to model the binary pixel values. The full architecture can be summarised as follows, where the parameters of the GatedConvTranspose2d, in order, denote the number of input channels, the number of output channels, kernel size, stride, padding and (optionally) the output padding:

- GatedConvTranspose2d(10, 64, 7, 1, 0)
- GatedConvTranspose2d(64, 64, 5, 1, 2)
- GatedConvTranspose2d(64, 32, 5, 2, 2, 1)
- GatedConvTranspose2d(32, 32, 5, 1, 2)
- GatedConvTranspose2d(32, 32, 5, 2, 2, 1)
- GatedConvTranspose2d(32, 32, 5, 1, 2)
- GatedConvTranspose2d(32, 1, 1, 1, 0)

C.1.3 PixelCNN++ decoder

We follow Alemi et al. [2018] in slightly modifying the work of Salimans et al. [2017] to function as a VAE decoder architecture. The latent $\mathbf{z}$ is added to the decoder via a conditioning mechanism in all the GatedResNet blocks. This mechanism projects the latent to the spatial dimensions of the feature maps that are the output of this block ($\mathbf{x_1}$ and $\mathbf{x_2}$) and and adds the projections to all channels identically before the gating mechanism. The operation can be described as:

$$\mathbf{y}_{\text{GatedResNet}} = (\mathbf{x_1} + \mathbf{V}^T\mathbf{z}) \odot \sigma(\mathbf{x_2} + \mathbf{W}^T\mathbf{z})$$

We use three down-sampling blocks ($28 \rightarrow 14 \rightarrow 7$) and three up-sampling blocks ($7 \rightarrow 14 \rightarrow 28$) with skip connections between blocks of equal spatial dimensionality. Each block consists of 2 GatedResNet units and the number of filters is set to 64. We adapt the output layer to output the parameters of the Bernoulli distribution over the spatial dimensions of the image (28 x 28).

C.2 PENN TREEBANK

C.2.1 Distil RoBERTa Encoder

For the encoder we use a transformer architecture, specifically a RoBERTa Encoder architecture Liu et al. [2019][3] and initialise with weights that are obtained by means of knowledge distillation Sanh et al. [2019].[4] We add a pooling layer that maps the output of the encoder to the parameters of the approximate posterior distribution.

C.2.2 Adapted Distil Roberta Decoder

For the decoder we use the same basis as for the encoder. We adapt its architecture following the work of Li et al. [2020] to incorporate the latent representations via two mechanisms: the attention mechanism and the embedding mechanism. For the former, the latent representation is mapped to the dimensionality of the hidden layers for every layer in the model and added via the attention mechanism in the form of key and value vectors. For the latter mechanism, the latent representation is simply projected to the dimensionality of the hidden layers and is summed with the initial hidden states of the model, right after embedding the tokens. This operation is the same for all positions in the sequence. At the output, a language model head is added to map the output of the RoBERTa block to the parameters of a Categorical distribution that models the token distributions per sequence position. Auto-regressive masking is used to prevent the model to have access to information beyond the current token position.

[3] We use the implementation of Huggingface described here: `https://huggingface.co/docs/transformers/model_doc/roberta`

[4] Specifically we use the weights from the `distil-roberta` checkpoint: `https://huggingface.co/distilroberta-base`

D LATENT STRUCTURE MODELS AND LPPD STATISTICS

D.1 GRAPHICAL MODELS

Table 3 shows the graphical models of the latent structure models used for our analysis.

MNIST	PTB		Latent
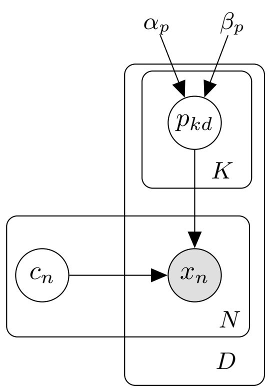	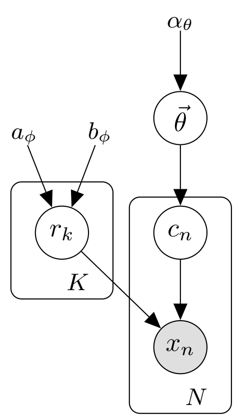	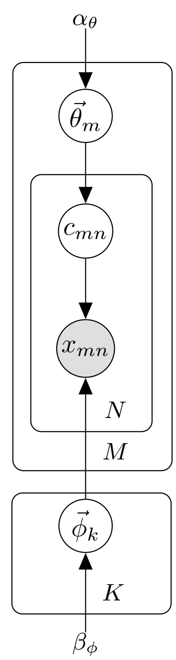	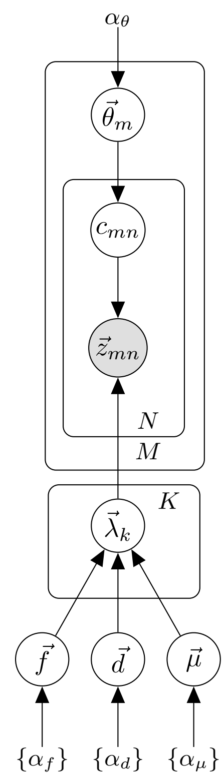
Digit identity	Sequence length	Topic structure	Prior structure

Table 3: This table shows the latent structure models described in Section 5.2 used to demonstrate the proposed evaluation methodology. The captions denote the latent structure that is captured by each individual model and is represented graphically by the latent variable c.

D.2 MODEL CHECKS

In the following sections we will provide material to assess goodness of fit of the latent structure models used in our analysis.

D.2.1 MNIST digit identity

In Figure 5 we show average digits sampled from the held out dataset next to average digits sampled from the posterior predictive of the MNIST digit identity model as presented in section 5 to assess its fit. In Figure 6 numerical posterior predictive checks are shown.

D.2.2 PTB sequence length

In Figure 7 histograms of the sampled lengths of the models trained on the Penn Treebank dataset are shown together with the true lengths. This is the raw data used for the sequence length latent structure model. Posterior predictive checks for this

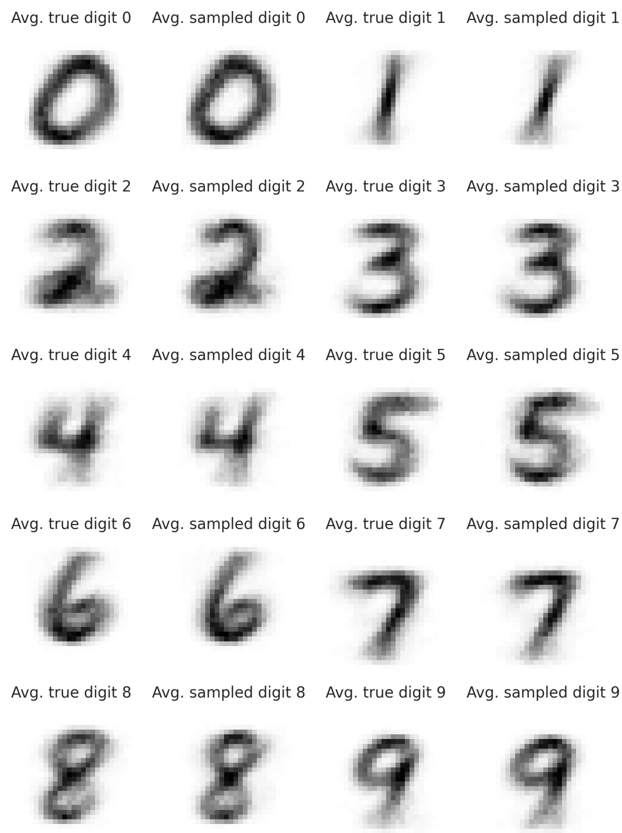

Figure 5: Average sampled digits from the held-out dataset are plotted next (left) to average sampled digits from the posterior predictive of the MNIST digit identity latent structure model (right).

latent structure model fit on the held out data are shown in Figure 8 and Figure 9.

D.2.3 PTB topics

Topic	Token 0	Token 1	Token 2	Token 3	Token 4	Token 5	Token 6	Token 7	Token 8	Token 9
0	market	stock	price	trading	investor	day	trader	future	index	buy
1	mr	say	big	dow	jones	dow_jones	one	point	world	going
2	test	mr	cancer	house	treatment	director	state	federal	whether	senate
3	million	share	year	billion	sale	earlier	quarter	company	rose	month
4	company	new	laboratory	operation	billion	corp	calif	loan	los	deficit
5	bond	rate	year	dollar	market	franc	bank	interest	billion	yield
6	company	inc	third	corp	president	executive	chief	co	third_quarter	unilab
7	new	york	new_york	stock	exchange	month	closed	trading	stock_exchange	yesterday
8	next	data	control	export	would	company	spending	year	computer	friday
9	mr	say	year	could	buyer	central	drug	old	time	would

Table 4: The top 10 tokens per topic as identified by the LDA topic model.

To choose the hyperparameters of the LDA topic model that is fit to the Penn Treebank data, we perform a hyperparameter experiment. To this end, we compute the per-token log likelihood bound and a sliding window topic coherence score (Gensim's `c_v`), using the held-out Penn Treebank data. Based on these results (visualised in Figure 10) we set `alpha` to 0.01 and set the number of topics to 10. Figures 11 shows an additional check to assess goodness of fit for the LDA model given these hyperparameters.

D.2.4 Latent space

In Figure 12 we plot the average posterior component sample for the latent analysis models.

D.3 FULL EXPERIMENTAL RESULTS LPPD STATISTICS

Full experimental results for the three type of statistics measured under the three latent structure models can be found in Figures 13, 14 and 15.

E INTRINSIC EVALUATION RESULTS

The full results as visualised in Figure 2 are listed in Tables 5 and 6 for the binarised MNIST and PTB experiments respectively.

F GROUPED MIXED MEMBERSHIP MODELS

To compare the statistic histograms across groups in a systematic way, we fit Dirichlet process mixed membership models to the scalar valued statistics with the group variable denoting the different experiments and control group. In total we fit 9 of these models for the three statistics across three latent structure models. We use a truncated Normal as family for the components and uniform priors for the location and scale parameters of these components. The number of components is 5 for both the statistics resulting from the sequence length model and topic model and 7 for the MNIST digit identity model.

Figures 16 – 24 depict posterior predictive samples for different groups under the analysis DP mixture models that are used to compare the statistics $T(x^*)$, $T(\tilde{x}^*)$ and $T(\tilde{x}^*|x^*)$ evaluated under the three latent structure models (the MNIST digit identity model, the Penn Treebank sequence length model and the Penn Treebank LDA topic model) for different groups.

G ESTIMATED DIVERGENCE TO CONTROL GROUP

In Figures 25 – 27 we plot full experimental results of the plots equivalent to those presented in Figure 4 in Section 5.

Decoder	Objective	λ_{FB}	β	λ_{MMD}	λ_{rate}	IW LL	ELBO	Rate	Distortion	MMD
CNN.T	BETA-VAE	-	0.00	-	-	-1908747.684	-1910785.802	1910706.699	79.108	0.265494
PixelCNN++	BETA-VAE	-	0.00	-	-	-236.732	-235.079	174.957	60.122	0.530988
CNN.T	INFO-VAE	-	-	100	10.0	-140.217	-157.334	3.218	154.116	0.000446
CNN.T	INFO-VAE	-	-	10	10.0	-139.367	-157.106	3.275	153.831	0.000721
CNN.T	INFO-VAE	-	-	1	10.0	-135.821	-155.290	3.412	151.878	0.000594
CNN.T	BETA-VAE	-	10.00	-	-	-123.197	-142.718	4.104	138.614	0.000462
CNN.T	INFO-VAE	-	-	10	0.1	-112.413	-115.687	36.708	78.979	0.055015
CNN.T	INFO-VAE	-	-	10	5.0	-111.122	-122.567	8.437	114.130	0.004309
CNN.T	INFO-VAE	-	-	10	0.5	-103.501	-106.251	24.296	81.955	0.042997
CNN.T	INFO-VAE	-	-	1	0.1	-102.699	-105.651	37.987	67.665	0.109114
CNN.T	INFO-VAE	-	-	10	2.0	-101.911	-107.297	14.748	92.550	0.009465
CNN.T	FB-VAE	40	-	-	-	-101.823	-104.936	37.671	67.265	0.131946
CNN.T	INFO-VAE	-	-	10	1.0	-101.392	-103.785	19.484	84.300	0.016348
CNN.T	INFO-VAE	-	-	100	0.1	-99.630	-102.594	34.361	68.233	0.003865
CNN.T	BETA-VAE	-	5.00	-	-	-99.506	-111.420	9.002	102.418	0.001213
CNN.T	INFO-VAE	-	-	100	5.0	-99.419	-111.431	9.074	102.356	0.001087
CNN.T	INFO-VAE	-	-	1	5.0	-96.905	-111.545	8.959	102.586	0.001620
CNN.T	FB-VAE	32	-	-	-	-96.250	-99.154	30.607	68.547	0.054848
CNN.T	BETA-VAE	-	0.25	-	-	-95.583	-98.752	30.788	67.964	0.054161
PixelCNN++	INFO-VAE	-	-	10	0.1	-92.755	-96.713	35.803	60.910	0.021386
PixelCNN++	INFO-VAE	-	-	1	0.1	-92.494	-96.655	46.089	50.566	0.063386
CNN.T	BETA-VAE	-	2.00	-	-	-92.004	-95.649	15.915	79.735	0.006296
CNN.T	BETA-VAE	-	0.50	-	-	-91.366	-95.277	25.682	69.595	0.021536
CNN.T	INFO-VAE	-	-	1	1.0	-91.075	-93.643	20.741	72.901	0.010445
CNN.T	INFO-VAE	-	-	100	0.5	-91.047	-94.688	25.119	69.568	0.002931
CNN.T	INFO-VAE	-	-	100	1.0	-90.987	-93.405	20.492	72.913	0.002752
CNN.T	INFO-VAE	-	-	1	2.0	-90.903	-95.517	15.738	79.779	0.004205
CNN.T	BETA-VAE	-	0.75	-	-	-90.609	-93.535	22.650	70.885	0.014209
CNN.T	FB-VAE	24	-	-	-	-90.534	-94.576	24.228	70.348	0.019529
CNN.T	FB-VAE	4	-	-	-	-90.221	-93.075	20.691	72.385	0.009502
CNN.T	FB-VAE	8	-	-	-	-90.140	-93.111	20.838	72.272	0.012566
CNN.T	FB-VAE	16	-	-	-	-89.955	-93.511	21.312	72.199	0.012732
CNN.T	INFO-VAE	-	-	100	2.0	-89.805	-95.291	15.892	79.399	0.002115
CNN.T	BETA-VAE	-	1.00	-	-	-89.767	-93.170	20.516	72.654	0.009939
CNN.T	INFO-VAE	-	-	1	0.5	-89.740	-94.728	25.616	69.112	0.020474
PixelCNN++	FB-VAE	40	-	-	-	-89.652	-91.937	38.192	53.746	0.088447
CNN.T	BETA-VAE	-	1.50	-	-	-88.192	-93.665	18.052	75.612	0.006233
PixelCNN++	BETA-VAE	-	0.25	-	-	-88.009	-90.369	38.595	51.773	0.026900
PixelCNN++	FB-VAE	32	-	-	-	-83.701	-86.769	31.107	55.661	0.024090
PixelCNN++	FB-VAE	24	-	-	-	-83.304	-84.196	23.840	60.356	0.008685
PixelCNN++	INFO-VAE	-	-	10	5.0	-83.249	-82.019	0.000	82.018	-0.000051
PixelCNN++	INFO-VAE	-	-	10	10.0	-83.124	-82.152	0.000	82.152	0.000044
PixelCNN++	INFO-VAE	-	-	10	2.0	-82.733	-81.971	0.000	81.970	-0.000009
PixelCNN++	INFO-VAE	-	-	10	0.5	-82.244	-82.234	0.002	82.232	0.000076
PixelCNN++	INFO-VAE	-	-	10	1.0	-82.243	-82.169	0.001	82.169	-0.000157
PixelCNN++	INFO-VAE	-	-	1	5.0	-81.965	-80.716	0.000	80.716	0.000060
PixelCNN++	BETA-VAE	-	0.50	-	-	-81.886	-84.875	26.952	57.923	0.006013
PixelCNN++	INFO-VAE	-	-	1	10.0	-81.783	-82.144	0.000	82.144	-0.000015
PixelCNN++	BETA-VAE	-	1.50	-	-	-81.690	-80.745	0.000	80.745	-0.000073
PixelCNN++	INFO-VAE	-	-	100	1.0	-81.587	-80.926	0.003	80.923	-0.000021
PixelCNN++	INFO-VAE	-	-	100	0.1	-81.552	-80.771	0.004	80.767	0.000193
PixelCNN++	INFO-VAE	-	-	100	5.0	-81.419	-80.846	0.003	80.843	0.000667
PixelCNN++	BETA-VAE	-	1.00	-	-	-81.165	-80.664	0.001	80.663	0.000035
PixelCNN++	INFO-VAE	-	-	100	10.0	-81.058	-81.975	0.001	81.974	-0.000118
PixelCNN++	INFO-VAE	-	-	100	2.0	-80.952	-80.756	0.011	80.744	0.000926
PixelCNN++	FB-VAE	16	-	-	-	-80.698	-81.895	16.927	64.968	0.002087
PixelCNN++	INFO-VAE	-	-	1	2.0	-80.670	-80.555	0.003	80.553	0.000333
PixelCNN++	INFO-VAE	-	-	1	0.5	-80.669	-84.514	26.190	58.324	0.003956
PixelCNN++	INFO-VAE	-	-	100	0.5	-80.658	-80.769	0.003	80.766	0.000000
PixelCNN++	BETA-VAE	-	2.00	-	-	-80.505	-80.817	0.000	80.817	0.000025
PixelCNN++	FB-VAE	4	-	-	-	-80.446	-80.548	5.755	74.794	0.000707
PixelCNN++	BETA-VAE	-	5.00	-	-	-80.228	-80.670	0.000	80.669	0.000144
PixelCNN++	INFO-VAE	-	-	1	1.0	-80.023	-80.621	0.000	80.620	0.000174
PixelCNN++	BETA-VAE	-	0.75	-	-	-79.370	-80.819	8.785	72.034	0.000669
PixelCNN++	BETA-VAE	-	10.00	-	-	-79.335	-80.604	0.000	80.604	-0.000003
PixelCNN++	FB-VAE	8	-	-	-	-78.865	-80.663	9.761	70.902	0.001080

Table 5: Full intrinsic evaluation results of experiments on Binarised MNIST dataset

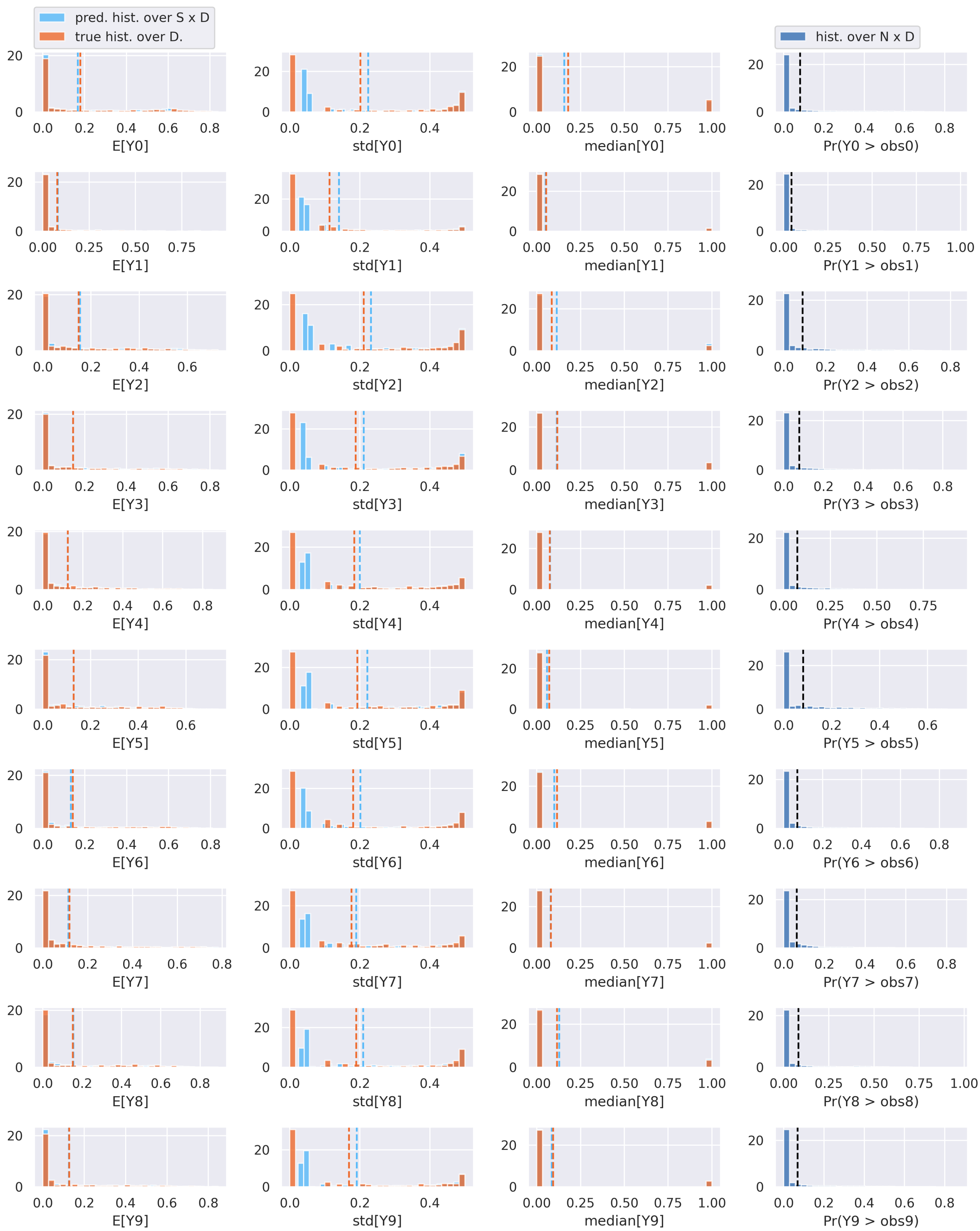

Figure 6: Posterior predictive checks for the MNIST digit identity latent structure model fit to the data, row-wise organised per digit group. From left to right it shows histograms over the mean, the standard deviation, the median and the probability that a sampled pixel value from the posterior predictive exceeds that of a sampled pixel from held out observations.

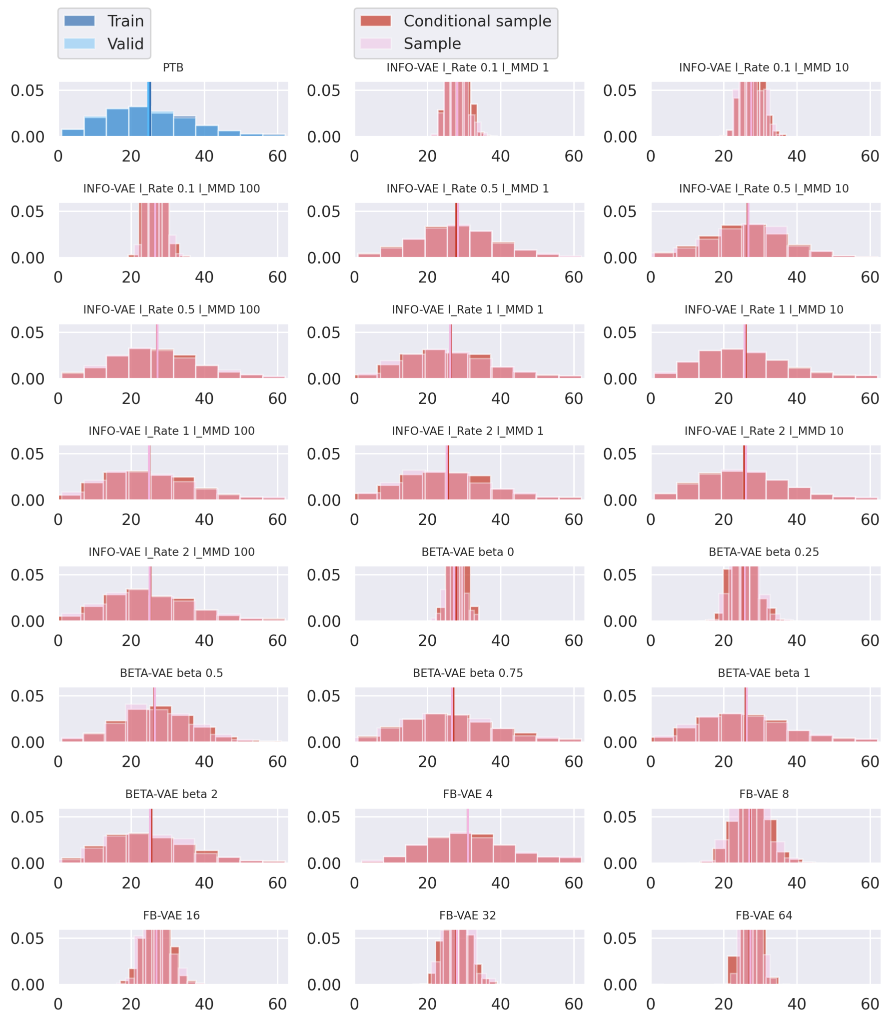

Figure 7: Sequence length histograms of model samples (pink and red hues) and data samples (blue hues).

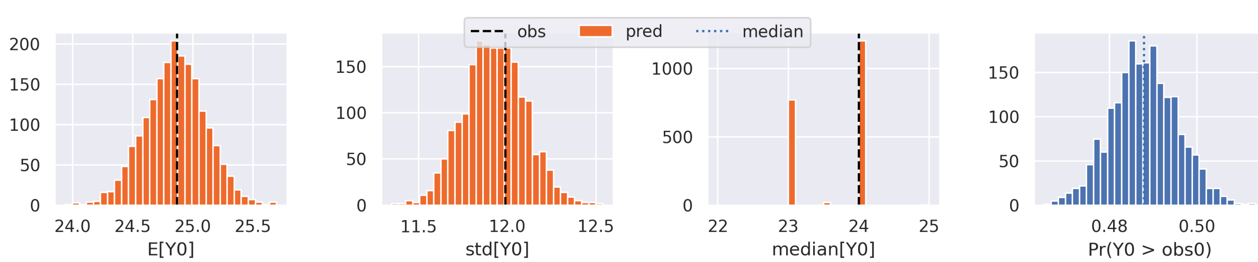

Figure 8: Posterior predictive checks for the sequence length latent structure model. From left to right it shows histograms over the mean, the standard deviation, the median and the probability that a sampled length value from the posterior predictive exceeds that of a sampled length from held out observations.

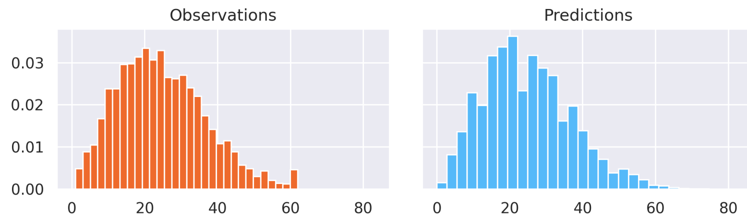

Figure 9: A histogram of sampled lengths from the held out Penn Treebank dataset (left) next to sampled lengths from the posterior predictive of the sequence length latent structure model (right).

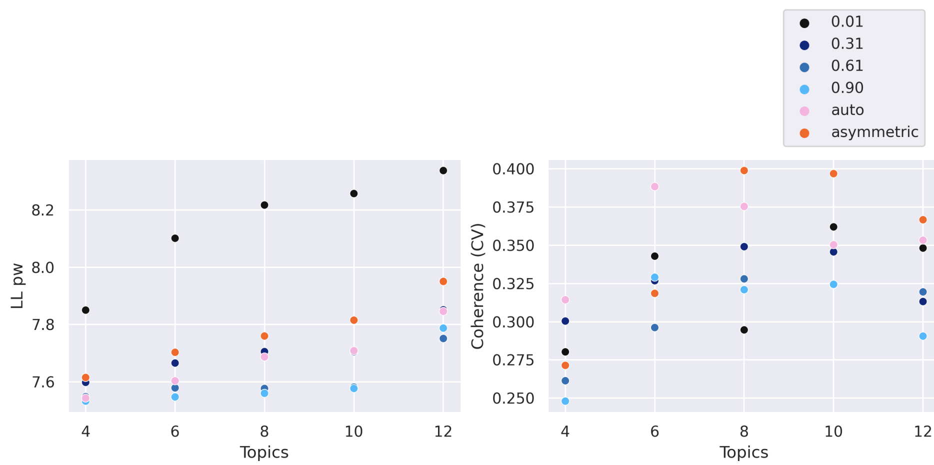

Figure 10: The per-token log likelihood bound and a sliding window topic coherence for different number of topics and different values for `alpha`.

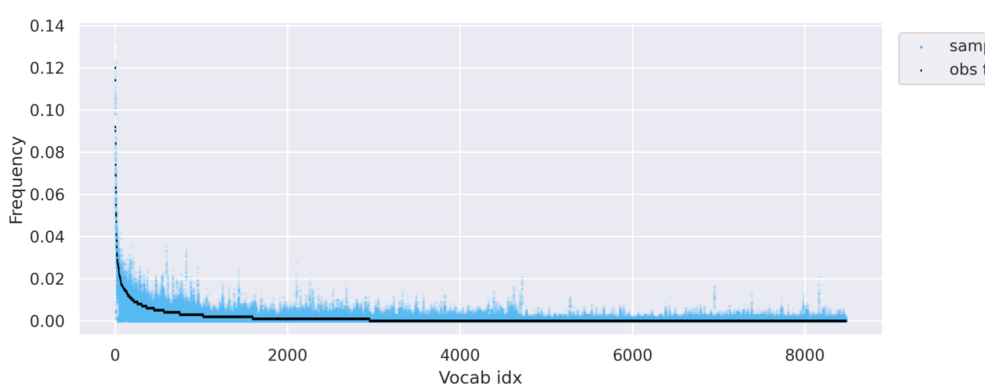

Figure 11: True sorted token frequencies of the Penn Treebank data set plotted against re-sampled sorted token frequencies sampled from the fitted LDA model.

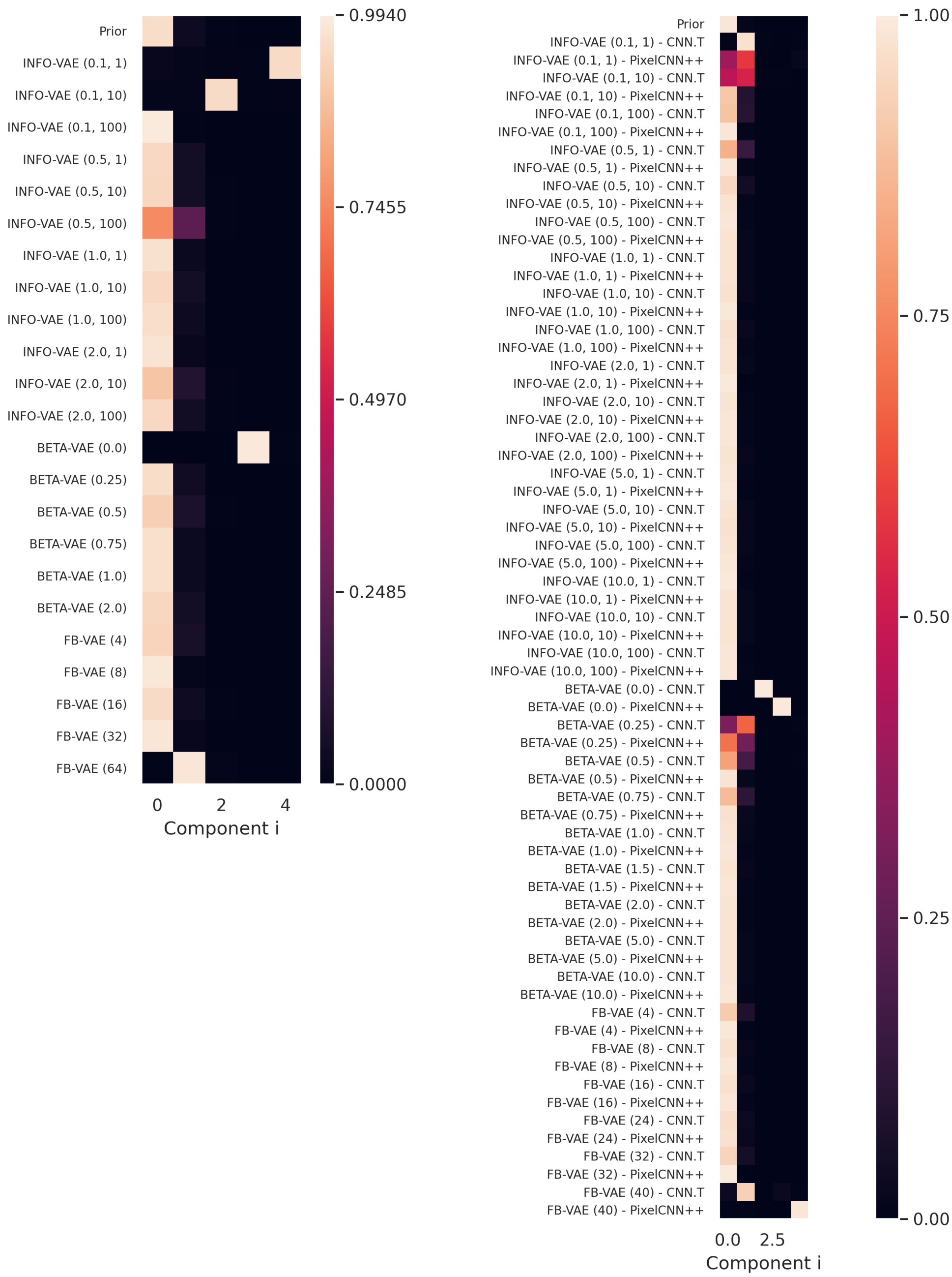

Figure 12: Sampled components from the posterior of the latent analysis models for all experiment groups and the control (data group). The left column shows the PTB experiments, right the MNIST experiments.

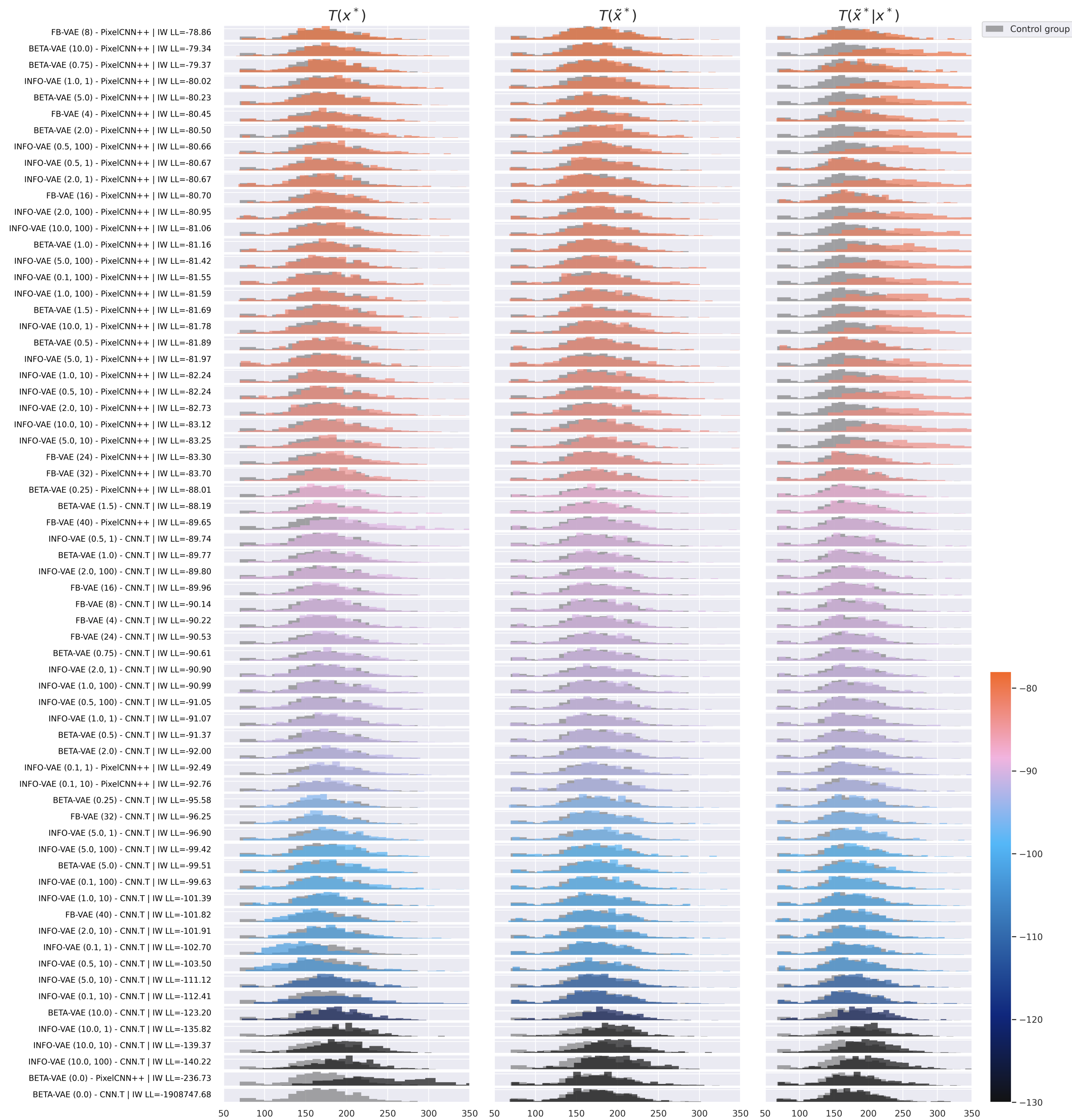

Figure 13: The three statistics $T(x^*)$, $T(\tilde{x}^*)$ and $T(\tilde{x}^*|x^*)$ based on the log posterior predictive density of the MNIST digit identity latent structure model of the experiments plotted against the respective control groups. The rows are ordered and coloured by an importance weighted estimate of the log likelihood (IW LL) of the VAEs on held-out data.

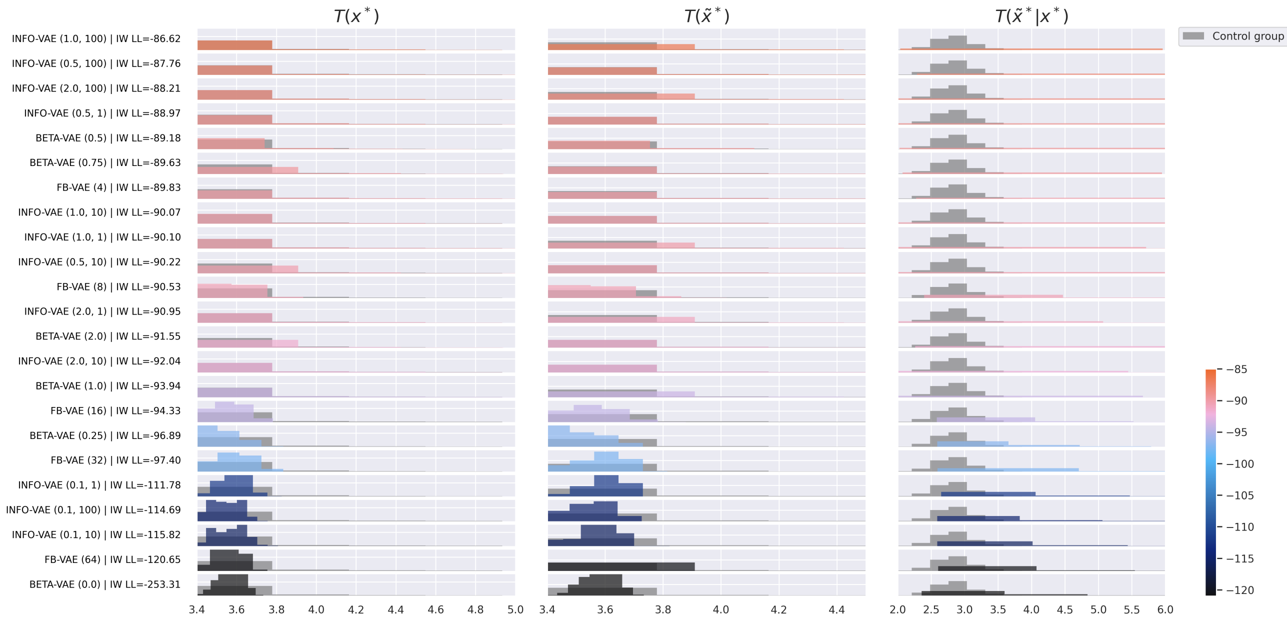

Figure 14: The three statistics $T(x^*)$, $T(\tilde{x}^*)$ and $T(\tilde{x}^*|x^*)$ based on the log posterior predictive density of the PTB sequence length latent structure model of the experiments plotted against the respective control groups. The rows are ordered and coloured by an importance weighted estimate of the log likelihood (IW LL) of the VAEs on held-out data.

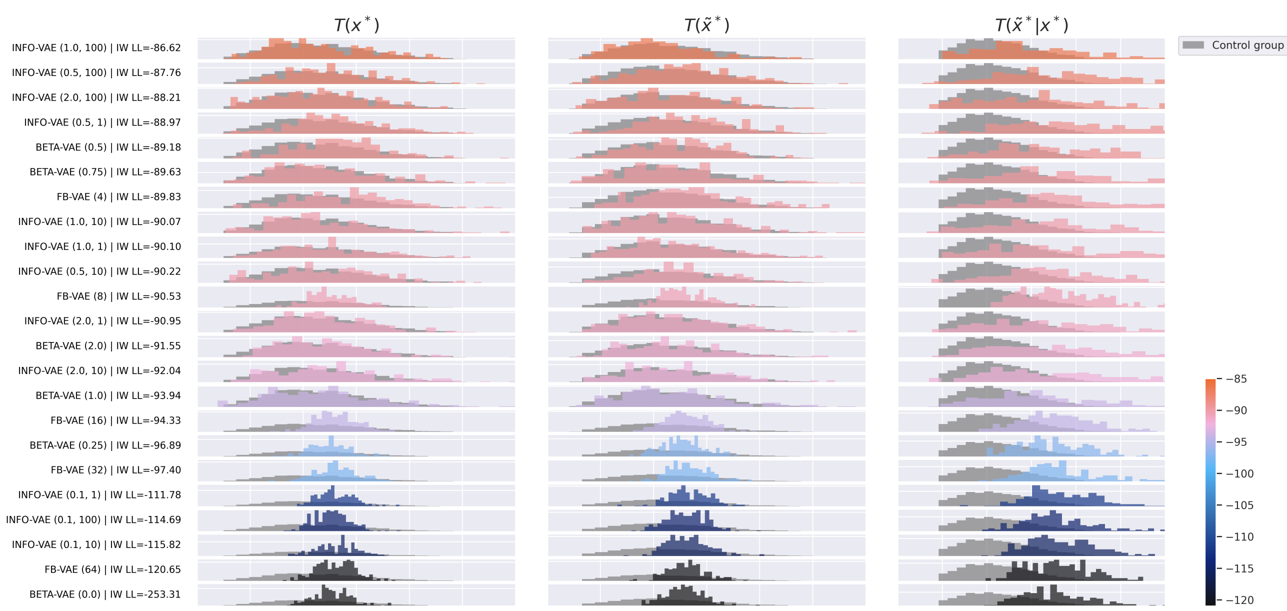

Figure 15: The three statistics $T(x^*)$, $T(\tilde{x}^*)$ and $T(\tilde{x}^*|x^*)$ based on the log posterior predictive density of the PTB topic latent structure model of the experiments plotted against the respective control groups. The rows are ordered and coloured by an importance weighted estimate of the log likelihood (IW LL) of the VAEs on held-out data.

Decoder	Objective	λ_{FB}	β	λ_{MMD}	λ_{rate}	IW LL	ELBO	Rate	Distortion	MMD
Distil roBERTa	BETA-VAE	-	0.000	-	-	-253.314	-262.025	199.762	62.263	0.004164
Distil roBERTa	FB-VAE	64	-	-	-	-120.653	-125.793	60.116	65.677	0.000889
Distil roBERTa	INFO-VAE	-	-	10	0.1	-115.817	-119.895	51.583	68.311	0.000932
Distil roBERTa	INFO-VAE	-	-	100	0.1	-114.690	-118.358	48.643	69.715	0.000672
Distil roBERTa	INFO-VAE	-	-	1	0.1	-111.780	-119.874	51.270	68.604	0.000934
Distil roBERTa	FB-VAE	32	-	-	-	-97.405	-103.309	30.311	72.998	0.000347
Distil roBERTa	BETA-VAE	-	0.25	-	-	-96.893	-101.637	26.318	75.319	0.000433
Distil roBERTa	FB-VAE	16	-	-	-	-94.325	-95.389	15.632	79.757	0.000246
Distil roBERTa	BETA-VAE	-	1.00	-	-	-93.939	-89.989	0.006	89.983	0.000011
Distil roBERTa	INFO-VAE	-	-	10	2.0	-92.038	-90.203	0.002	90.202	-0.000003
Distil roBERTa	BETA-VAE	-	2.00	-	-	-91.553	-90.596	0.001	90.595	0.000004
Distil roBERTa	INFO-VAE	-	-	1	2.0	-90.949	-90.400	0.001	90.399	0.000003
Distil roBERTa	FB-VAE	8	-	-	-	-90.527	-92.318	8.047	84.271	0.000134
Distil roBERTa	INFO-VAE	-	-	10	0.5	-90.219	-91.485	4.573	86.912	0.000085
Distil roBERTa	INFO-VAE	-	-	1	1.0	-90.100	-90.172	0.004	90.168	0.000018
Distil roBERTa	INFO-VAE	-	-	10	1.0	-90.073	-90.215	0.005	90.210	-0.000010
Distil roBERTa	FB-VAE	4	-	-	-	-89.834	-91.519	3.829	87.690	0.000075
Distil roBERTa	BETA-VAE	-	0.75	-	-	-89.629	-90.604	0.021	90.583	0.000017
Distil roBERTa	BETA-VAE	-	0.50	-	-	-89.176	-91.301	4.669	86.632	0.000131
Distil roBERTa	INFO-VAE	-	-	1	0.5	-88.973	-91.410	4.468	86.943	0.000075
Distil roBERTa	INFO-VAE	-	-	100	2.0	-88.214	-90.436	0.002	90.434	0.000004
Distil roBERTa	INFO-VAE	-	-	100	0.5	-87.757	-91.146	3.669	87.477	0.000156
Distil roBERTa	INFO-VAE	-	-	100	1.0	-86.616	-90.574	0.004	90.570	0.000018

Table 6: Full intrinsic evaluation results of experiments on Penn Treebank dataset

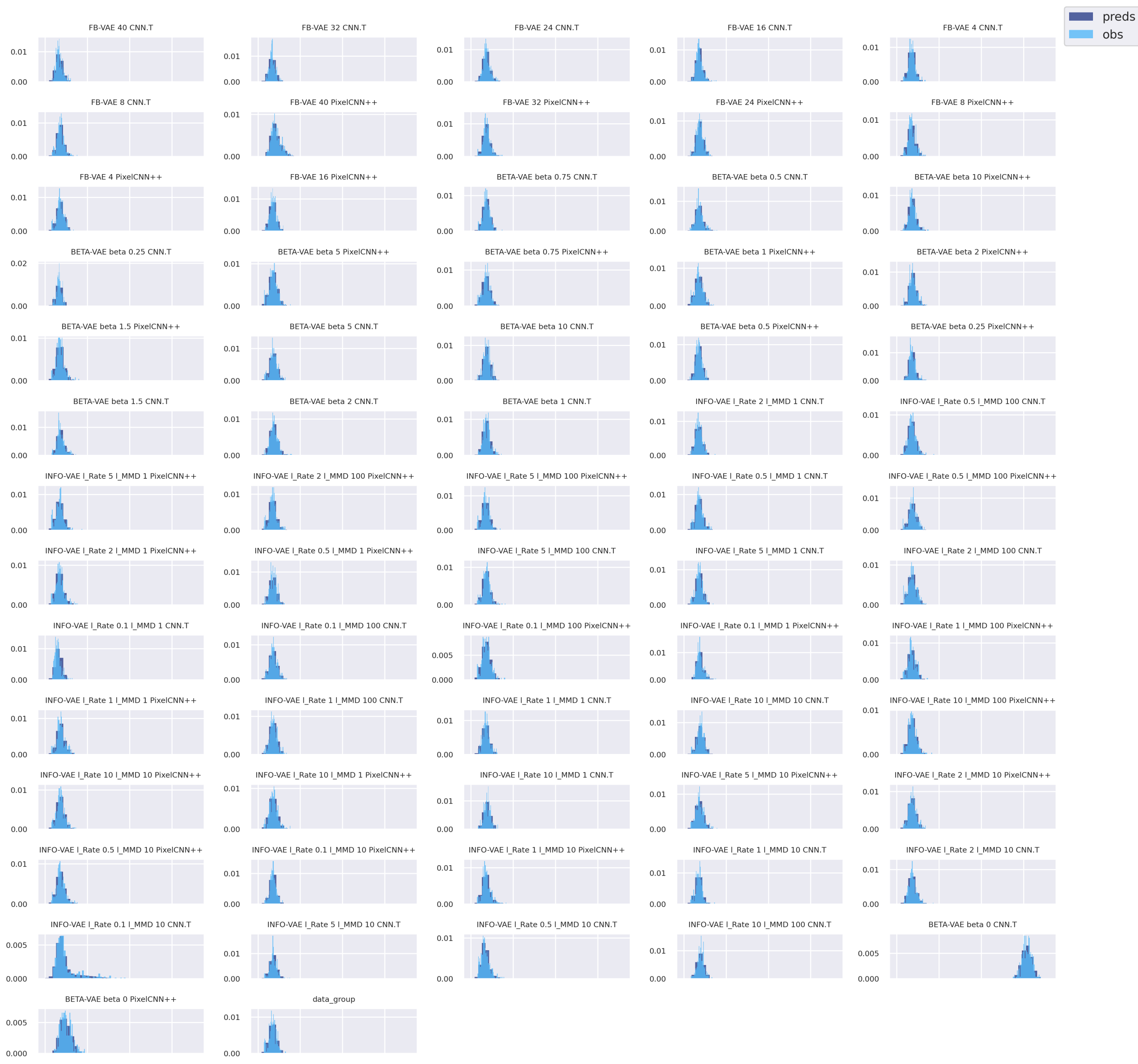

Figure 16: Posterior predictive samples (preds) versus observations (obs) of the $T(x^*)$ statistic assessed under the MNIST digit identity latent structure model as modelled by the DP mixture model.

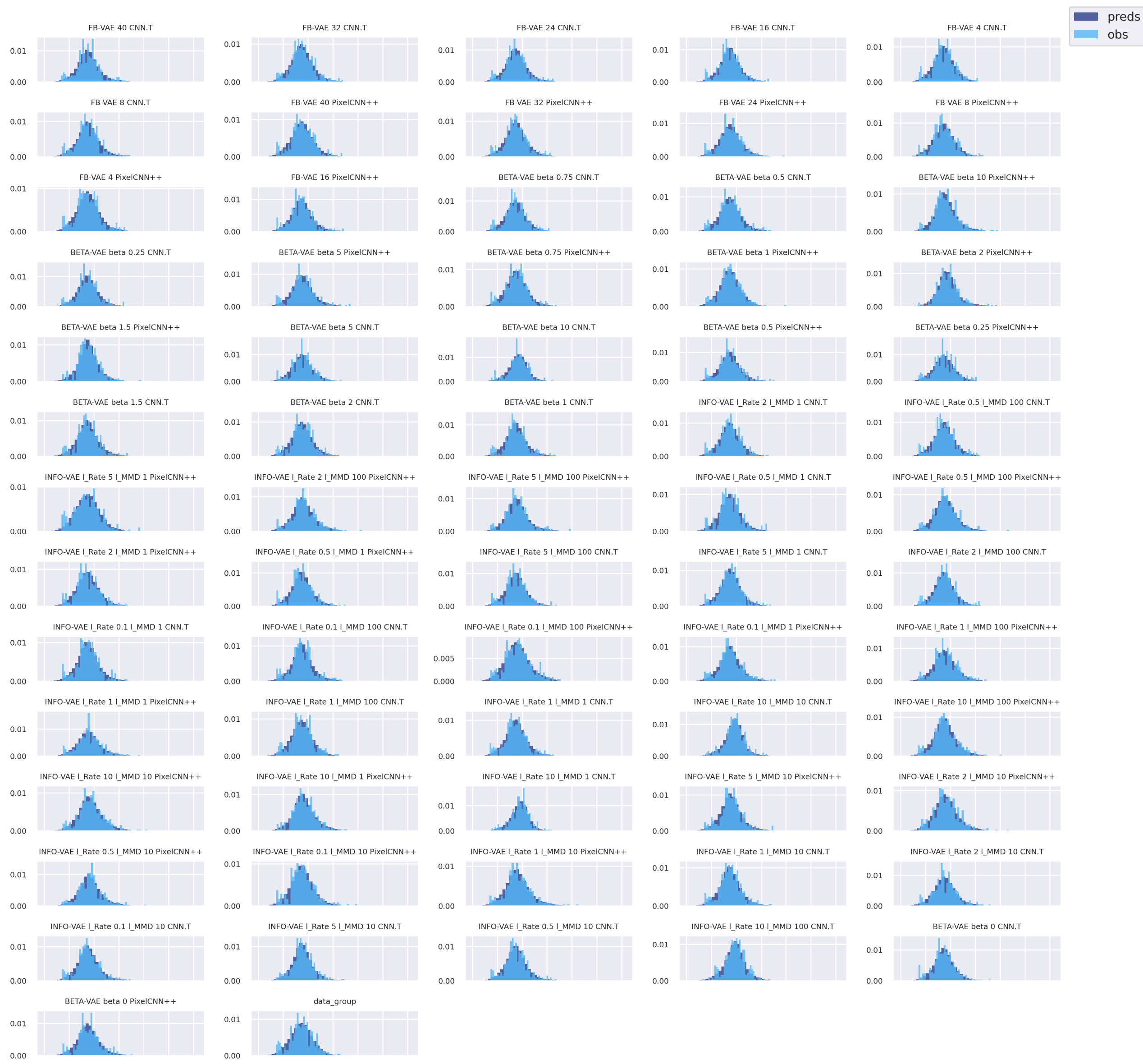

Figure 17: Posterior predictive samples (preds) versus observations (obs) of the $T(\tilde{x}^*)$ statistic assessed under the MNIST digit identity latent structure model as modelled by the DP mixture model.

Figure 18: Posterior predictive samples (preds) versus observations (obs) of the $T(\tilde{x}^*|x^*)$ statistic assessed under the MNIST digit identity latent structure model as modelled by the DP mixture model.

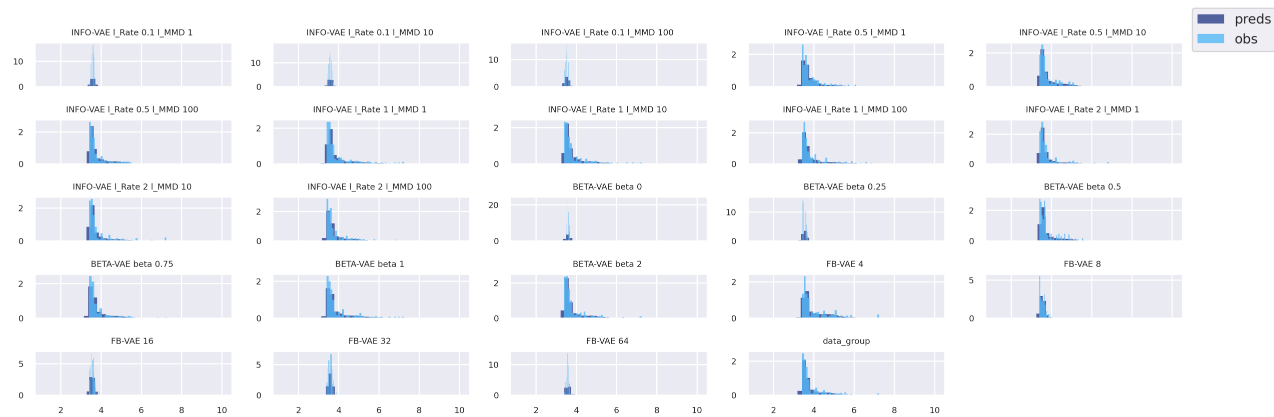

Figure 19: Posterior predictive samples (preds) versus observations (obs) of the $T(x^*)$ statistic assessed under the Penn Treebank sequence length latent structure model as modelled by the DP mixture model.

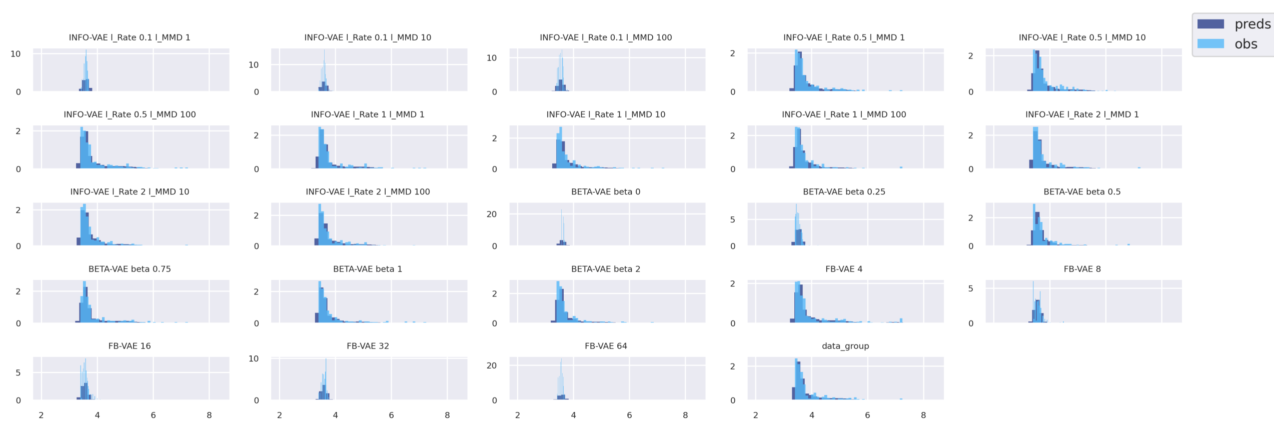

Figure 20: Posterior predictive samples (preds) versus observations (obs) of the $T(\tilde{x}^*)$ statistic assessed under the Penn Treebank sequence length latent structure model as modelled by the DP mixture model.

Figure 21: Posterior predictive samples (preds) versus observations (obs) of the $T(\tilde{x}^*|x^*)$ statistic assessed under the Penn Treebank sequence length latent structure model as modelled by the DP mixture model.

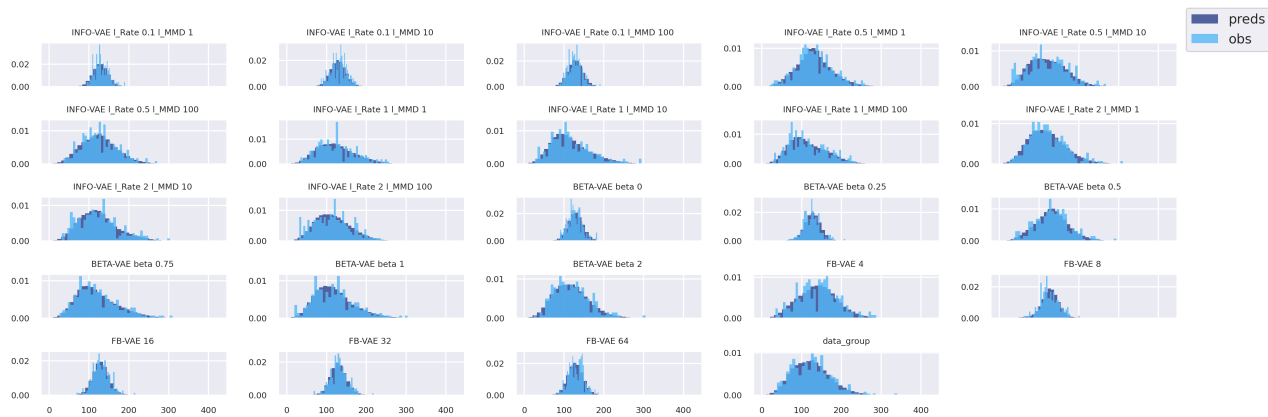

Figure 22: Posterior predictive samples (preds) versus observations (obs) of the $T(x^*)$ statistic assessed under the Penn Treebank topic latent structure model as modelled by the DP mixture model.

Figure 23: Posterior predictive samples (preds) versus observations (obs) of the $T(\tilde{x}^*)$ statistic assessed under the Penn Treebank topic latent structure model as modelled by the DP mixture model.

Figure 24: Posterior predictive samples (preds) versus observations (obs) of the $T(\tilde{x}^*|x^*)$ statistic assessed under the Penn Treebank topic latent structure model as modelled by the DP mixture model.

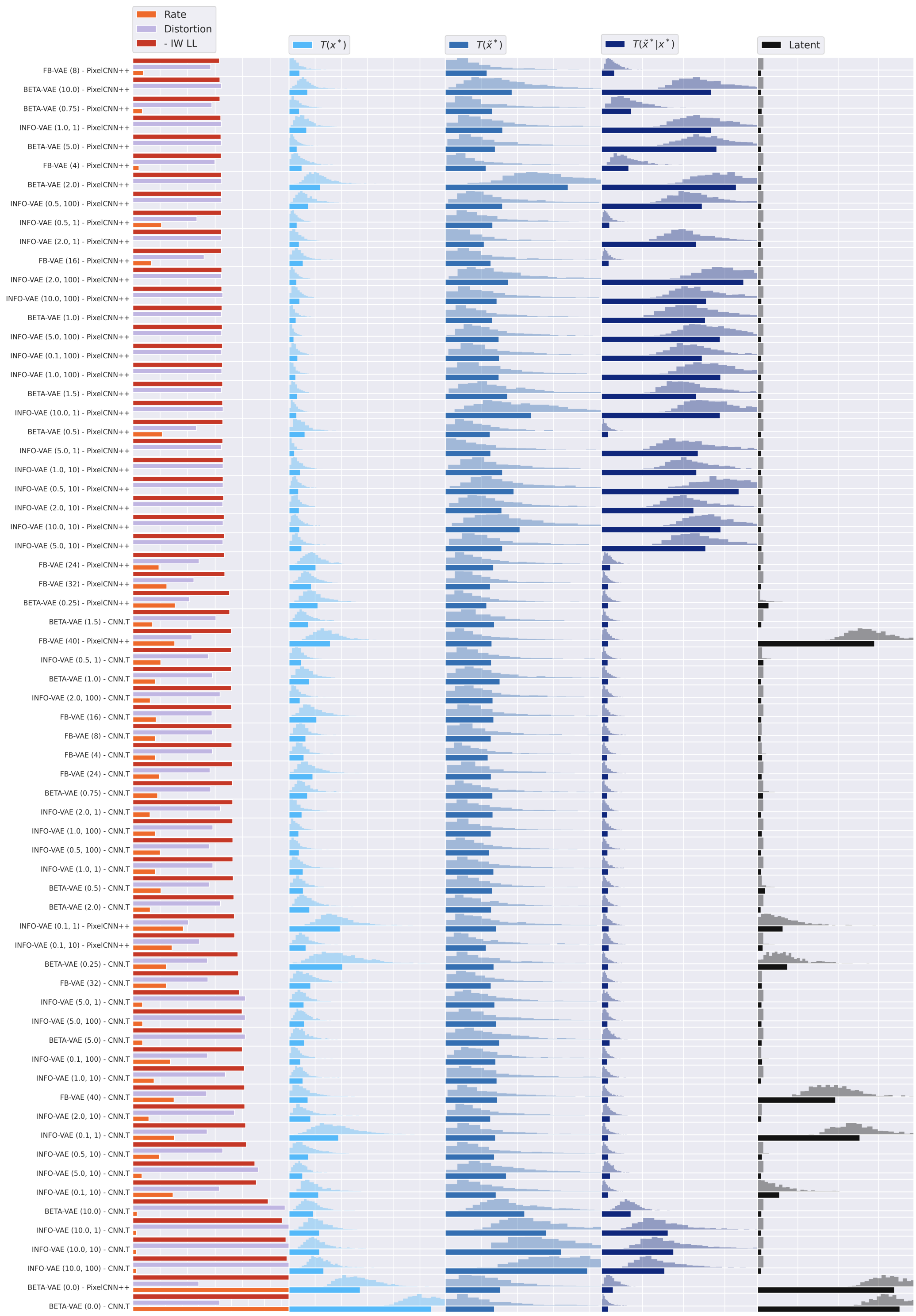

Figure 25: Full experimental results for the control group divergence analysis for the MNIST digit identity structure model. The left most column shows the intrinsic evaluation metrics for reference. The middle three columns show estimated divergences from the control group under our analysis model. The right most column shows the control group divergence under the latent analysis model. The horizontal bars denote the average value of the sampled divergences plotted as histograms. The experiments are labelled with the objectives according to the following format: INFOVAE (λ_{rate}, λ_{MMD}), BETAVAE (β) and FBVAE (λ_{FB}). We additionally distinguish between decoder types used: CNN.T or PixelCNN++.

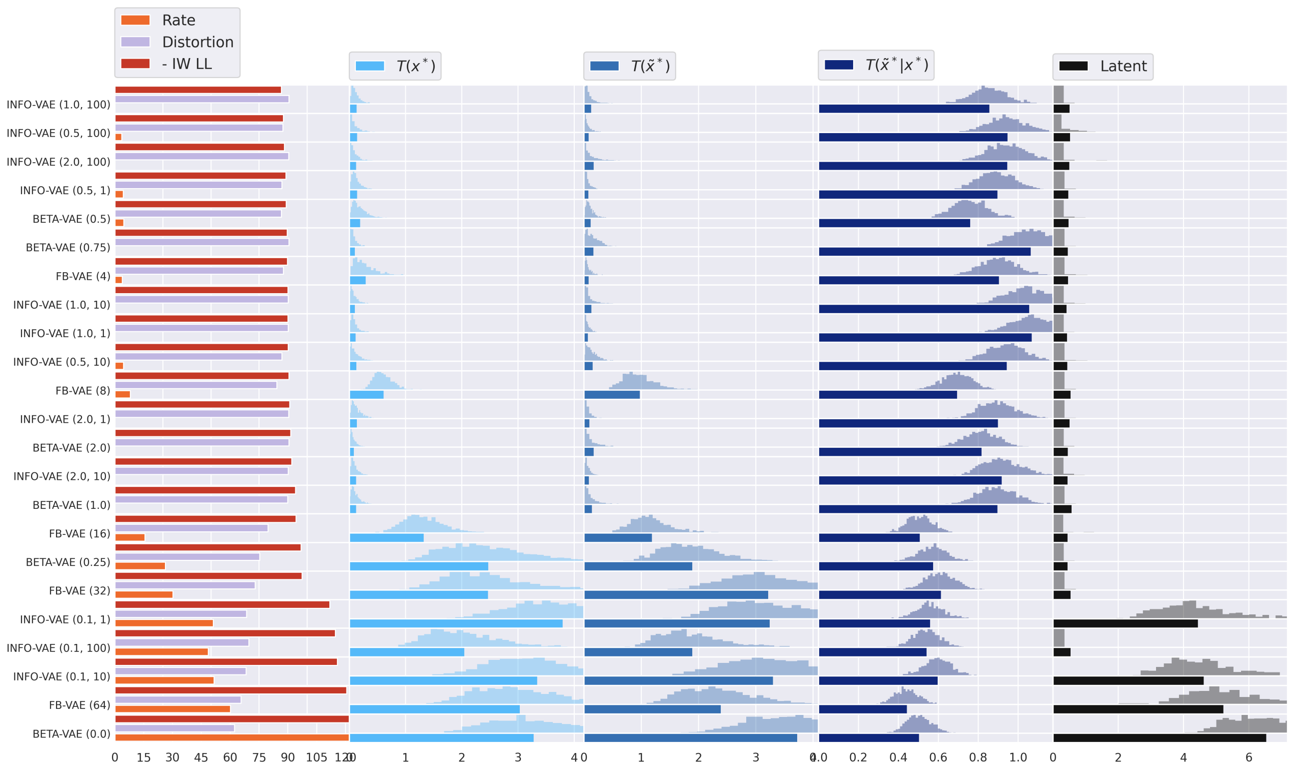

Figure 26: Full experimental results for the control group divergence analysis for the PTB sequence length latent structure model. The left most column shows the intrinsic evaluation metrics for reference. The middle three columns show estimated divergences from the control group under our analysis model. The right most column shows the control group divergence under the latent analysis model. The horizontal bars denote the average value of the sampled divergences plotted as histograms. The experiments are labelled with the objectives according to the following format: INFOVAE (λ_{rate}, λ_{MMD}), BETAVAE (β) and FBVAE (λ_{FB}).

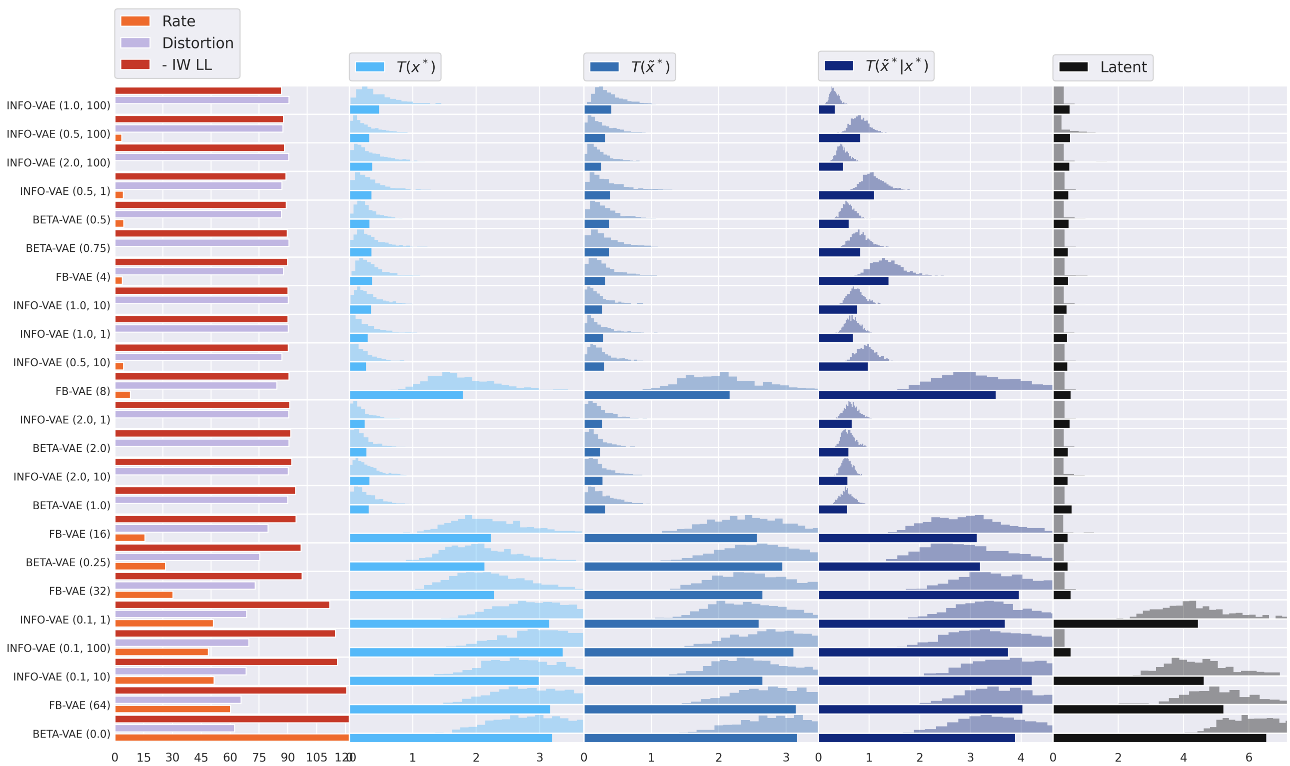

Figure 27: Full experimental results for the control group divergence analysis for the PTB topic structure model. The left most column shows the intrinsic evaluation metrics for reference. The middle three columns show estimated divergences from the control group under our analysis model. The right most column shows the control group divergence under the latent analysis model. The horizontal bars denote the average value of the sampled divergences plotted as histograms. The experiments are labelled with the objectives according to the following format: INFOVAE (λ_{rate}, λ_{MMD}), BETAVAE (β) and FBVAE (λ_{FB}).